

Integration of continuous-time dynamics in a spiking neural network simulator

Jan Hahne^{1†*}, David Dahmen^{2†}, Jannis Schuecker^{2†}, Andreas Frommer¹, Matthias Bolten³, Moritz Helias^{2,4} and Markus Diesmann^{2,4,5}

¹School of Mathematics and Natural Sciences
Bergische Universität Wuppertal
Wuppertal, Germany

²Institute of Neuroscience and Medicine (INM-6)
Institute for Advanced Simulation (IAS-6)
JARA BRAIN Institute I
Jülich Research Centre
Jülich, Germany

³Institut für Mathematik
Universität Kassel
Kassel, Germany

⁴Department of Physics
Faculty 1
RWTH Aachen University
Aachen, Germany

⁵Department of Psychiatry, Psychotherapy and Psychosomatics
Medical Faculty
RWTH Aachen University
Aachen, Germany

†These authors contributed equally

*Correspondence to: Jan Hahne
Bergische Universität Wuppertal
42097 Wuppertal, Germany
hahne@math.uni-wuppertal.de

Abstract

Contemporary modeling approaches to the dynamics of neural networks consider two main classes of models: biologically grounded spiking neurons and functionally inspired rate-based units. The unified simulation framework presented here supports the combination of the two for multi-scale modeling approaches, the quantitative validation of mean-field approaches by spiking network simulations, and an increase in reliability by usage of the same simulation code and the same network model specifications for both model classes. While most efficient spiking simulations rely on the communication of discrete events, rate models require time-continuous interactions between neurons. Exploiting the conceptual similarity to the inclusion of gap junctions in spiking network simulations, we arrive at a reference implementation of instantaneous and delayed interactions between rate-based models in a spiking network simulator. The separation of rate dynamics from the general connection and communication infrastructure ensures flexibility of the framework. We further demonstrate the broad applicability of the framework by considering various examples from the literature ranging from random networks to neural field models. The study provides the prerequisite for interactions between rate-based and spiking models in a joint simulation.

Keywords

rate models, spiking neural network simulator, stochastic (delay) differential equations, waveform relaxation, NEST

1 Introduction

Over the past decades, multiple strategies of neural network modeling have emerged in computational neuroscience. Functionally inspired top-down approaches that aim to understand the computation in neural networks typically describe neurons or neuronal populations in terms of continuous variables, e.g. firing rates (Hertz et al., 1991; Schöner et al., 2015). Rate-based models originate from the seminal works by Wilson & Cowan (1972) and Amari (1977) and were introduced as a coarse-grained description of the overall activity of large-scale neuronal networks. Being amenable to mathematical analyses and exhibiting rich dynamics such as multistability, oscillations, traveling waves, and spatial patterns (Coombes, 2005; Roxin et al., 2005; Bressloff, 2012), rate-based models have fostered progress in the understanding of memory, sensory and motor processes (Kilpatrick, 2014). Particular examples include visuospatial working memory (Camperi & Wang, 1998; Laing et al., 2002), decision making (Usher & McClelland, 2001; Bogacz et al., 2006, 2007), perceptual rivalry (Laing & Chow, 2002; Wilson, 2003), geometric visual hallucination patterns (Ermentrout & Cowan, 1979; Bressloff et al., 2001), ocular dominance and orientation selectivity (Ben-Yishai et al., 1995; Bressloff & Cowan, 2003; Stevens et al., 2013), spatial navigation (Samsonovich & McNaughton, 1997), and movement preparation (Erlhagen & Schöner, 2002). On the brain scale, rate models have been used to study resting-state activity (Deco et al., 2011) and hierarchies of time scales (Chaudhuri et al., 2015). Ideas from functional network models have further inspired the field of artificial neuronal networks in the domain of engineering (Haykin, 2009).

In contrast, bottom-up approaches explicitly model individual neurons, employing biophysically grounded spiking neuron models that simulate the time points of action potentials. These models can explain a variety of salient features of microscopic neural activity observed *in vivo*, such as spike-train irregularity (Softky & Koch, 1993; van Vreeswijk & Sompolinsky, 1996; Amit & Brunel, 1997; Shadlen & Newsome, 1998), membrane-potential fluctuations (Destexhe & Paré, 1999), asynchronous firing (Brunel, 2000; Ecker et al., 2010; Renart et al., 2010; Ostojic, 2014), correlations in neural activity (Gentet et al., 2010; Okun & Lampl, 2008; Helias et al., 2013), self-sustained activity (Ohbayashi et al., 2003; Kriener et al., 2014), rate distributions across neurons (Griffith & Horn, 1966; Koch & Fuster, 1989; Roxin et al., 2011) and across laminar populations (Potjans & Diesmann, 2014), as well as resting state activity (Deco & Jirsa, 2012).

Simulation of rate-based models goes back to the works by Grossberg (1973), McClelland & Rumelhart (1981), Feldman & Ballard (1982), and the PDP group (Rumelhart et al., 1986). Various specialized tools have developed since then (O'Reilly, 2014), such as *PDP++* (McClelland & Rumelhart, 1989; O'Reilly et al., 2000), the *Neural Simulation Language* (Weitzenfeld et al., 2002), *emergent* (O'Reilly et al., 2012), the *MIIND* simulator (De Kamps et al., 2008), the simulation platform *DANA* (Rougier & Fix, 2012), *TheVirtualBrain* (Sanz Leon et al., 2013), *Topographica* (Bednar, 2009) and the *Neural Field Simulator* (Nichols & Hutt, 2015). Similarly, efficient simulators for spiking neural networks have evolved with different foci ranging from detailed neuron morphology (NEURON (Carnevale & Hines, 2006), GENESIS (Bower & Beeman, 2007)) to an abstraction of neurons to a single point in space (NEST (Bos et al., 2015), BRIAN (Goodman & Brette, 2013), see Brette et al., 2007, for a review). Such open-source software supports maintainability, reproducibility, and exchangeability of models and code, as well as community driven development. However, these tools are restricted to either rate-based or spike-based models only.

The situation underlines that bottom-up and top-down strategies are still mostly disjoint and a major

challenge in neuroscience is to form a bridge between the spike- and rate-based models (Abbott et al., 2016), and, more generally, between the fields of computational neuroscience and cognitive science. From a practical point of view, a common simulation framework would allow the exchange and the combination of concepts and code between the two descriptions and trigger interaction between the corresponding communities. This is in particular important since recent advances in simulation (Djurfeldt et al., 2008; Hines et al., 2008; Kumar et al., 2010; Hines et al., 2011; Helias et al., 2012; Kunkel et al., 2014) and computing technology (Jülich Supercomputing Centre, 2015) enable full-density bottom-up models of complete circuits (Potjans & Diesmann, 2014; Markram et al., 2015). In particular, it has become feasible to build spiking models (Schmidt et al., 2016) that describe the same macroscopic system as the rate-based descriptions (Chaudhuri et al., 2015).

Mean-field theories pave the way to relate spiking and rate-based descriptions of neuronal dynamics (Deco et al., 2008). Population density methods using Fokker-Planck theory can be used to determine stationary state activities of spiking networks (Siegert, 1951; Brunel, 2000). The dynamics of rate fluctuations around this background activity can be obtained using linear response theory (Brunel & Hakim, 1999; Lindner et al., 2005; Ostojic & Brunel, 2011; Trousdale et al., 2012; Grytskyy et al., 2013; Schuecker et al., 2015), moment expansions for mode decompositions of the Fokker-Planck operator (Mattia & Del Giudice, 2002, 2004; Deco et al., 2008), or other specific ansatzes (Montbrió et al., 2015). An alternative derivation of rate-based dynamics aims at a closure of equations for synaptic currents of spiking networks in a coarse-graining limit by replacing spiking input with the instantaneous firing rate (Bressloff, 2012). Using field-theoretical methods (Buice & Chow, 2013) that were originally developed for Markovian network dynamics (Buice & Cowan, 2007; Buice et al., 2010) allows a generalization of this approach to fluctuations in the input (Bressloff, 2015). In any case, the cascade of simplifications from the original spiking network to the rate-based model involves a combination of approximations which are routinely benchmarked in comparative simulations of the two models. A unified code base that features both models would highly simplify these benchmarks rendering duplication of code obsolete.

Rate neurons typically represent populations of spiking neurons. Thus, a hybrid model, employing both types of neuron models in a multi-scale modeling approach, would contain a relatively large number of spiking neurons compared to the number of rate units. Furthermore a downscaling of a spiking network cannot be performed without changing the dynamics (van Albada et al., 2015) and thus it is crucial that a common simulation framework is able to handle real-sized spiking networks. In addition, the employed mean-field theories exploit the large number of neurons in biological networks. In fact, they are strictly valid only in the thermodynamic limit $N \rightarrow \infty$ (Helias et al., 2014). Therefore, in the above mentioned benchmarks, the spiking networks are typically large. Thus, a common simulation framework should be optimized for spiking neurons rather than rate-based models.

Current spiking network simulators solve the neuronal dynamics in a distributed and parallel manner. They exploit the point-event like nature of the spike interaction between neurons, for example in event-based simulation schemes. The latter, however, can not be employed in the context of rate-based models which require continuous interactions between units. Spiking point-neuron models furthermore interact in a delayed fashion. The delays mimic the synaptic transmission and the propagation times along axons and dendrites. For the duration of the minimal delay d_{\min} in a network, the dynamics of all neurons is decoupled. Hence, during d_{\min} , the neurons can be updated independently without requiring information from other neurons. Distributed processes therefore need to communicate spikes only after this period (Morrison et al., 2005). Due to considerable latencies associated with each communication, this scheme significantly improves performance and scalability of current simulators. In contrast, rate based-models (see Bressloff, 2012, and references therein) consider instantaneous interactions between neurons. A priori, this requires communication of continuous state variables between neurons at each time step.

The present study provides the concepts and a reference implementation for the embedding of continuous-time dynamics in a spiking network simulator. In order to exploit existing functionality we choose as a platform the open source simulation code NEST (Gewaltig & Diesmann, 2007; Bos et al., 2015) which is scalable software that can be used on machines ranging from laptops to supercomputers. The software is utilized by a considerable user community and equipped with a Python interface, support for the construction of complex networks, and mechanisms to shield the neuroscientist from the difficulties of handling a model description, potentially including stochastic components, in a distributed setting (Morrison et al., 2005; Plesser et al., 2015). Within this framework we introduce an iterative numerical solution scheme that reduces communication between compute nodes. The scheme builds on the waveform-relaxation technique (Lelarasme, 1982) already employed for gap-junction interactions (Hahne et al., 2015).

Our study begins with a brief review of numerical solution schemes for ordinary and stochastic (delay) differential equations in Sec. 2 and their application to neural networks in Sec. 2.2. Subsequently, we develop the concepts for embedding rate-based network models into a simulation code for spiking networks, adapt the waveform-relaxation scheme, and detail an extendable implementation framework for neuron models in terms of C++ templates Sec. 2.3. In Sec. 3, different numerical schemes are evaluated as well as the scalability of our

reference implementation. We illustrate the applicability of the framework to a broad class of network models on the examples of a linear network model (Grytskyy et al., 2013), a nonlinear network model (Sompolinsky et al., 1988; Goedeke et al., 2016), a neural field model (Roxin et al., 2005), and a mean-field description (Wong & Wang, 2006) of the stationary activity in a model of the cortical microcircuit (Potjans & Diesmann, 2014; Schuecker et al., 2016). Straight-forward generalizations are briefly mentioned at the end of the Results section, before the work concludes with the Discussion in Sec. 4. The technology described in the present article will be made available with one of the next major releases of the simulation software NEST as open source. The conceptual and algorithmic work is a module in our long-term collaborative project to provide the technology for neural systems simulations (Gewaltig & Diesmann, 2007).

2 Material and methods

Rate-based single neuron and population models are described in terms of differential equations that often include delays and stochastic elements. Before we turn to the implementation of such models in computer code (Sec. 2.3) we review how such systems are mathematically solved and in particular how the stochastic elements are commonly interpreted with the aim to avoid an ad hoc design. A stochastic differential equation (SDE) is defined by the corresponding stochastic integral equation. Let $W(t)$ denote a Wiener process, also called Standard Brownian motion. For the initial condition $X(t_0) = X_0$ an Itô-SDE in its most general form satisfies

$$X(t) = X_0 + \int_{t_0}^t a(s, X(s)) ds + \int_{t_0}^t b(s, X(s)) dW(s), \quad (1)$$

where the second integral is an Itô integral

$$\int_{t_0}^t Y(s) dW(s) := \lim_{n \rightarrow \infty} \sum_{i=1}^n Y_{i-1} \cdot (W_i - W_{i-1})$$

with $Y_i = Y(t_0 + i \cdot \frac{t-t_0}{n})$ and $W_i = W(t_0 + i \cdot \frac{t-t_0}{n})$. Alternatively, the second integral can be chosen as a Stratonovich integral, indicated by the symbol \circ ,

$$\int_{t_0}^t Y(s) \circ dW(s) := \lim_{n \rightarrow \infty} \sum_{i=1}^n \frac{Y_{i-1} + Y_i}{2} (W_i - W_{i-1})$$

which approximates $Y(s)$ with the mid-point rule. In this case, the corresponding SDE is called a Stratonovich-SDE. We refer to Kloeden & Platen (1992) and Gardiner (2004) for a derivation and a deeper discussion on the differences between the two types of stochastic integrals. In the case of additive noise ($b(t, X(t)) = b(t)$) the Itô and Stratonovich integrals coincide. If furthermore the noise is constant ($b(t, X(t)) = \sigma = \text{const.}$) the integrals can be solved analytically

$$\int_{t_0}^t \sigma dW(s) = \int_{t_0}^t \sigma \circ dW(s) = \lim_{n \rightarrow \infty} \sigma \cdot \sum_{i=1}^n (W_i - W_{i-1}) = \sigma \cdot (W(t) - W(t_0))$$

with $W(t) - W(t_0) \sim \mathcal{N}(0, t - t_0)$. In the following, we focus on Itô-SDEs only. The differential notation corresponding to (1) reads

$$dX(t) = a(t, X(t)) dt + b(t, X(t)) dW(t) \quad (2)$$

and denotes an informal way of expressing the integral equation. Another widely used differential notation, called the Langevin form of the SDE, is mostly employed in physics. It reads

$$\frac{dX(t)}{dt} = a(t, X(t)) + b(t, X(t)) \xi(t), \quad (3)$$

where $\xi(t)$ is a Gaussian white noise with $\langle \xi(t) \rangle = 0$ and $\langle \xi(t) \xi(t') \rangle = \delta(t - t')$. Using the Fokker-Planck equation one obtains

$$\int_0^t \xi(t') dt' = W(t),$$

which is a paradox, as one can also show that $W(t)$ is not differentiable (Gardiner, 2004, Chapter 4). Mathematically speaking this means that (3) is not strictly well-defined. The corresponding stochastic integral equation

$$X(t) = X_0 + \int_{t_0}^t a(s, X(s)) ds + \int_{t_0}^t b(s, X(s)) \xi(s) ds,$$

however, can be interpreted consistently with (1) as $dW(t) \equiv \xi(t)dt$.

2.1 Approximate numerical solution of SDEs. Similar to ordinary differential equations most stochastic differential equations cannot be solved analytically. Neuroscience therefore relies on approximate numerical schemes to obtain the solution of a given SDE. This section presents some basic numerical methods. Let Δt denote the fixed step size, $t_k = t_0 + k\Delta t$ the grid points of the discretization for $k = 0, \dots, n$, and X_k the approximation for $X(t_k)$ obtained by the numerical method, at which X_0 is the given initial value. We consider systems of N stochastic differential equations

$$dX(t) = a(t, X(t)) dt + b(t, X(t)) dW(t) \quad (4)$$

with initial condition $X(t_0) = X_0$. Here, $X(t) = (X^1(t), \dots, X^N(t))$ and $W(t) = (W^1(t), \dots, W^N(t))$ denote N -dimensional vectors and $a : \mathbb{R}^N \rightarrow \mathbb{R}^N$ and $b : \mathbb{R}^N \rightarrow \mathbb{R}^N$ are N -dimensional functions. $W(t)$ is an N -dimensional Wiener process, i.e., the components $W^i(t)$ are independent and identically distributed.

Euler-Maruyama. The Euler-Maruyama method is a generalization of the forward Euler method for ordinary differential equations (ODE). Accordingly, it approximates the integrands in (1) with their left-sided values. The update formula reads

$$X_{k+1} = X_k + a(t_k, X_k) \cdot \Delta t + b(t_k, X_k) \cdot \Delta W_k \quad (5)$$

with $\Delta W_k = W(t_{k+1}) - W(t_k) \sim \mathcal{N}(0, \Delta t)$ for $k = 0, \dots, n-1$.

Semi-implicit Euler. The (semi-)implicit Euler method is a generalization of the backwards Euler method for ODEs. The update formula reads

$$X_{k+1} = X_k + a(t_{k+1}, X_{k+1}) \cdot \Delta t + b(t_k, X_k) \cdot \Delta W_k \quad (6)$$

with $\Delta W_k \sim \mathcal{N}(0, \Delta t)$ for $k = 0, \dots, n-1$. The resulting scheme requires the solution of a system of nonlinear algebraic equations. Standard techniques for the solution of the system are Newton iteration and fixed-point iteration (Kelley, 1995). The method is sometimes called semi-implicit, because the function b is still evaluated at (t_k, X_k) instead of (t_{k+1}, X_{k+1}) . However, a fully implicit Euler scheme for SDEs is not practicable (see Kloeden & Platen (1992), Chapter 9.8) and thus the term implicit Euler usually refers to the semi-implicit method.

Exponential Euler. The exponential Euler method relies on the assumption that $a(t, X(t))$ consists of a linear part and a nonlinear remainder, i.e.,

$$a(t, X(t)) = A \cdot X(t) + f(t, X(t))$$

with $A \in \mathbb{R}^{N \times N}$. The idea is to solve the linear part exactly and to approximate the integral of the nonlinear remainder and the Itô integral with an Euler-like approach. Variation of constants for (4) yields

$$X(t) = e^{A(t-t_0)} X_0 + \int_{t_0}^t e^{A(t-s)} f(s, X(s)) ds + \int_{t_0}^t e^{A(t-s)} b(s, X(s)) dW(s).$$

There are several versions of stochastic exponential Euler methods that differ in the approximation of the integral. Unfortunately a standardized nomenclature to distinguish the methods is so far missing. The simplest approach, sometimes named stochastic Lawson-Euler scheme (e.g. in Komori & Burrage, 2014), approximates the integrands with their left-sided values:

$$X_{k+1} = e^{A\Delta t} X_k + e^{A\Delta t} f(t_k, X_k) \cdot \Delta t + e^{A\Delta t} b(t_k, X_k) \cdot \Delta W_k.$$

More advanced schemes approximate the nonlinear part by keeping $f(s, X(s))$ constant for $[t_0, t)$ and solving the remaining integral analytically

$$\int_{t_0}^t e^{A(t-s)} f(s, X(s)) ds \approx \int_{t_0}^t e^{A(t-s)} f(t_0, X(t_0)) ds = A^{-1}(e^{A(t-t_0)} - I) \cdot f(t_0, X(t_0)).$$

Here I denotes the $N \times N$ identity matrix. The same technique can be used for the Itô integral

$$\int_{t_0}^t e^{A(t-s)} b(s, X(s)) dW(s) \approx \int_{t_0}^t e^{A(t-s)} b(t_0, X(t_0)) dW(s). \quad (7)$$

For a single SDE, Shoji (2011) proposed a method where the remaining integral $\int_{t_0}^t e^{a(t-s)} dW(s)$ with $a \in \mathbb{R}$ is approximated by $\int_{t_0}^t \alpha dW(s)$, such that $\alpha \in \mathbb{R}$ is chosen to minimize the mean-square error. This results in a similar approximation as for the nonlinear part. Komori & Burrage (2014) adapted this approach for systems of SDEs. The scheme reads

$$X_{k+1} = e^{A\Delta t} X_k + A^{-1}(e^{A\Delta t} - I) \cdot f(t_k, X(t_k)) + \frac{1}{\Delta t} \cdot A^{-1}(e^{A\Delta t} - I) \cdot b(t_k, X_k) \cdot \Delta W_k.$$

Alternatively, calculating the variance of $X(t)$ within the approximation (7), amounts to (Adamu, 2011)

$$\text{Var}(X(t)) = b(t_0, X(t_0))^2 \cdot \text{Var}\left(\int_{t_0}^t e^{A(t-s)} dW(s)\right) = b(t_0, X(t_0))^2 \cdot A^{-1} \left(\frac{e^{2A(t-t_0)} - I}{2}\right).$$

The corresponding scheme reads

$$X_{k+1} = e^{A\Delta t} X_k + A^{-1}(e^{A\Delta t} - I) \cdot f(t_k, X(t_k)) + \sqrt{A^{-1} \left(\frac{e^{2A\Delta t} - I}{2}\right)} \cdot b(t_k, X_k) \cdot \eta_k \quad (8)$$

with $\eta_k \sim \mathcal{N}(0, 1)$ and yields the exact solution of the system if $a(t, X(t)) = A \cdot X(t)$ and $b(t, X(t)) = \text{const.}$, since $X(t)$ has Gaussian statistics in this case (Risken, 1996). Therefore in the following we exclusively employ (8) and just refer to it as the stochastic exponential Euler scheme. For more detailed reviews on the different stochastic exponential Euler methods we refer to (Adamu, 2011) and (Komori & Burrage, 2014).

2.2 Network of rate models. We here consider networks of N rate-based model neurons where each neuron receives recurrent input from the network. The system fulfills the Itô-SDEs

$$\tau^i dX^i(t) = \left[-X^i(t) + \mu^i + \phi \left(\sum_{j=1}^N w^{ij} \psi(X^j(t - d^{ij})) \right) \right] dt + \sqrt{\tau^i} \sigma^i dW^i(t) \quad i = 1, \dots, N \quad (9)$$

with possibly nonlinear input-functions $\phi(x)$ and $\psi(x)$, connection weights w^{ij} , mean input μ^i , and optional delays $d^{ij} \geq 0$. The corresponding Fokker-Planck equation shows that the parameter $\sigma^i \geq 0$ controls the variance of $X^i(t)$ and the time constant $\tau^i > 0$ its temporal evolution. For readability, from here on we omit neuron indices for σ, τ, μ , and d . The considered class of rate models only contains additive noise. Therefore, as noted above, the system (9) can be written as Stratonovich-SDEs without the need for change in the employed numerical methods. For an illustrative purpose we explicitly state the different explicit solution schemes for the network dynamics (9) with $d = 0$. The Euler-Maruyama update step reads

$$X_{k+1}^i = X_k^i + \left[-X_k^i + \mu + \phi \left(\sum_{j=1}^N w^{ij} \psi(X_k^j) \right) \right] \frac{1}{\tau} \Delta t + \frac{1}{\sqrt{\tau}} \sigma \Delta W_k^i. \quad (10)$$

For nonlinear $\phi(x)$ or $\psi(x)$ the exponential Euler update step is

$$X_{k+1}^i = e^{-\Delta t/\tau} X_k^i + (1 - e^{-\Delta t/\tau}) \left[\mu + \phi \left(\sum_{j=1}^N w^{ij} \psi(X_k^j) \right) \right] + \sqrt{\frac{1}{2}(1 - e^{-2\Delta t/\tau})} \sigma \eta_k^i \quad (11)$$

with $\eta_k^i \sim \mathcal{N}(0, 1)$. As $A = -I$ is a diagonal matrix, the exponential Euler scheme does not rely on a matrix exponential, but decomposes into N equations with scalar exponential functions. Note that with a linear choice, $\phi(x) = \psi(x) = x$, the system of SDEs can be written in matrix notation

$$\tau dX(t) = [A \cdot X(t) + \mu] dt + \sqrt{\tau} \sigma dW(t) \quad i = 1, \dots, N \quad (12)$$

with $A = -I + W$ and $W = (w^{ij})_{N \times N}$. Here the stochastic exponential Euler scheme (8) yields the exact solution of the system.

The numerical schemes presented in Sec. 2.1 are developed for SDEs ($d = 0$), but can analogously be used for stochastic delay differential equations (SDDEs) ($d > 0$), if the delay d is a multiple of the step size Δt . For the calculation of the approximation X_{k+1}^i in time step $k + 1$ the recurrent input is then evaluated from $X_{k-\frac{d}{\Delta t}}^j$, i.e. from $\frac{d}{\Delta t}$ steps earlier.

2.3 Implementation in spiking network simulation code. This section describes the embedding of rate-based models (Sec. 2.2) in a simulation code for spiking neuronal networks. Examples how to create, connect and record activity from rate models will be made available with the release of our reference implementation of the continuous-time dynamics in the simulation code NEST.

The software architecture for rate models is based on existing concepts: Morrison et al. (2005) describe distributed buffers for the storage of delayed interactions and the technique to consistently generate random numbers in a distributed setting, and Hahne et al. (2015) introduce so called `SecondaryEvents`, that allow the communication of any kind of data between pairs of neurons. These components are designed to be compatible with the parallel and distributed operation of a simulation kernel for spiking neuronal networks, ensuring an efficient use of clusters and supercomputers (Helias et al., 2012). This allows researchers to easily scale up network sizes to more realistic number of neurons. The highly parallelizable structure of modern simulation codes for spiking neuronal networks, however, also poses restrictions on the utilizable numerical methods.

2.3.1 Restrictions. Parallelization for spiking neuronal networks is achieved by distributing neurons over compute nodes. Since the dynamics of spiking neurons (in the absence of gap junctions) is decoupled for the duration of the minimal synaptic delay d_{\min} of the connections in the network, the states of the neurons can be propagated independently for this time interval. Thus it is sufficient to specify solvers on the single-neuron level. The spike times, i.e. the mediators of interaction between neurons, are then communicated in steps of d_{\min} . In contrast, in the case of interactions via gap junctions (Hahne et al., 2015) or rates, the single-neuron dynamics depends on continuous state variables, membrane potential or rate, of other neurons. These continuous variables need to be communicated and the mechanism for this is the `SecondaryEvent` introduced in the gap-junction framework by Hahne et al. (2015).

Furthermore, the global connectivity of the network is unknown to the single neuron. The neuron object sends and receives events handled by the network manager on the compute node harboring the neuron. However, the network manager only knows the incoming connections of the neurons on the compute node.

This structure makes it impossible to employ the implicit Euler scheme (6) with Newton iteration, which would require the simultaneous solution of a system of nonlinear algebraic equations with information distributed over all compute nodes. It is however possible to use implicit schemes with fixed-point iteration. To this end, the corresponding scheme needs to be formulated as a fixed-point iteration on the single-neuron level and the updated influences of other neurons have to be communicated in every iteration. The gap junction framework by Hahne et al. (2015) already specifies an iterative method to advance the state of the network by one time step with global accuracy control. Therefore, we investigate in Sec. 3.1 if for rate-based network models the payoff of an implicit scheme is large enough to justify the additional effort of an iterative solver.

The restricted knowledge of connectivity also limits the usage of the exponential Euler method. In the case of a linear rate model, we are not able to add the influence from all other rate neurons to the matrix A in (12), because most of these connections are unknown at the single-neuron level. Therefore, we use the exponential Euler method with $A = -I$ resulting in the update formula (11). This also has the benefit of avoiding the need to numerically evaluate a general matrix exponential as A is a diagonal matrix (see Sec. 2.2 for details).

2.3.2 Implementation. This section describes the additional data structure required for the implementation of rate-based models. As a result of the previous section and our analysis of the numerical schemes in Sec. 3 we restrict the discussion to the exponential Euler method where we assume $A = -I$ and identify $\Delta t = h$ with h denoting the global computation step size (Morrison et al., 2005). We have to distinguish the cases of connections with delay ($d > 0$) and connections without delay ($d = 0$). The former case is similar to spiking interaction: assuming a connection from neuron i to neuron j , the rate of neuron i needs to be available at neuron j after $\frac{d}{h}$ additional time steps. This can be ensured if the delay of the connection is considered in the calculation of the minimal delay d_{\min} that determines the communication interval. After communication the rate values are stored in a ring buffer of neuron j until they are due (Morrison & Diesmann, 2008). In the case of an instantaneous connection, the rate of neuron i at time t_0 needs to be known at time t_0 at the process which updates neuron j from t_0 to $t_0 + h$. Therefore, communication in every step is required for instantaneous rate connections, i.e. setting $d_{\min} = h$.

Due to the conceptual differences between instantaneous and delayed interactions (for the conceptual difference in the case of spiking interaction see Morrison & Diesmann, 2008) we define two different connection types and associated events: The connection type for connections with delay is called `delay_rate_connection` and is associated with the new `SecondaryEvent` type `DelayRateNeuronEvent`. Connections without delay are implemented with the connection type `rate_connection` with the corresponding secondary event `RateNeuronEvent`.

The template class `rate_neuron_ipn` provides a base implementation for rate models of category (9). In this implementation neurons can handle both `DelayRateNeuronEvent` and `RateNeuronEvent` allowing for

gain model	$\phi(x)$ or $\psi(x)$
lin_rate	x
tanh_rate	$\tanh(g \cdot x)$ with $g \in \mathbb{R}$
thresholdlin_rate	$g \cdot (x - \theta) \cdot H(x - \theta)$ with $g \in \mathbb{R}$

Table 1: **Template-derived rate-based neuron models.** The table shows the gain functions of the rate-based neuron models available in the NEST reference implementation. The name of a particular neuron model is formed by `<gain model>_ipn`.

simultaneous use of instantaneous and delayed connections. To represent the nonlinearities $\phi(x)$ and $\psi(x)$ the class contains an object `gain_` the type of which is determined by the template parameter `TGainfunction`. The ending `ipn` indicates input noise, as the noise directly enters the r.h.s. of (9). A constant boolean class member `linear_summation_` of `rate_neuron_ipn` determines if the nonlinearity expressed by the operator `()` of the object `gain_` should be interpreted as $\phi(x)$ (true) or $\psi(x)$ (false). The respective other function is assumed to be the identity function and the default setting for `linear_summation_` is true. While to our knowledge this implementation covers the majority of neuron models, the evaluation of the boolean parameter `linear_summation_` in every update step of each neuron could be improved in terms of efficiency if the type of nonlinearity would be decided upon at compile time. In the present architecture this would, however, result in twice as many template instances for a given set of gain functions. With the future capabilities of code generation (Plotnikov et al., 2016) in mind it might be beneficial to elevate the constant boolean member object to a constant template parameter to allow compilers efficient preprocessing and at the same time profit from the code reliability achievable by modern C++ syntax. The present base implementation reduces the effort of creating a specific rate model of category (9) to the specification of an instance of the template class `TGainfunction`. Afterwards the actual neuron model can be defined with a simple typedef like e.g.

```
typedef rate_neuron_ipn< nest::gainfunction_lin_rate > lin_rate_ipn;
```

Table 1 gives an overview of rate models of the NEST reference implementation. These models serve as a reference for the implementation of customized neuron models. Activity of rate neurons can be recorded using the `multimeter` and the recordable `rate_`.

2.3.3 Waveform-relaxation techniques. The instantaneous connections between rate-based models requires communication in every time step, which impairs the performance and scalability. On supercomputers communication is particularly expensive, because it is associated with a considerable latency. Therefore, we also study an alternative iterative approach based on waveform-relaxation techniques that allows us to use communication on a coarser time grid. As outlined above, in a simulator for spiking neuronal networks the communication intervals are defined by the minimal delay d_{\min} in the network. For simulations with instantaneous connections only, we attempt to reduce the communication load by setting the minimal delay to an arbitrary user specified value given by the parameter `wfr_comm_interval` (see Table 2). In case of additional delayed connections, the actual communication interval for waveform relaxation then follows as $\min(d_{\min}, \text{wfr_comm_interval})$. For details on waveform-relaxation methods and their application in the neuroscience context we refer to Hahne et al. (2015). Originally these methods were developed (Lelarsmee, 1982) and investigated (see e.g. Miekkala & Nevanlinna, 1987) for ODEs. More recently waveform relaxation methods have also been analyzed for SDEs (Schurz & Schneider, 2005) and successfully applied to large systems of SDEs (Fan, 2013).

Fig. 1B illustrates the concept of the iterative approach in contrast to the standard procedure in panel A. The iterative approach requires the repeated solution of all time steps in the communication interval and converges to the solution obtained with the standard approach (Fig. 1A). The iteration terminates when a user chosen convergence tolerance `wfr_tol` (see Table 2) is met. If the method needs less than d_{\min}/h iterations, the approach reduces the overall number of communications required to obtain the solution. In conclusion, the avoidance of communication in every step comes for the price of additional computational load.

The coupling of neurons via gap junctions is instantaneous and continuous in time and thus constitutes a very similar problem to the rate dynamics. In order to combine gap junctions with spiking dynamics Hahne et al. (2015) already devised an iterative technique. The dynamics of a neuron model supporting gap junctions is solved with an adaptive step-size ODE-solver, routinely carrying out several steps of the employed numerical method within one global computation time step h . The communication of a cubic interpolation of the membrane potential provides the solver with additional information, resulting in a more accurate solution than the one obtained from the standard approach. For rate-based models this approach is however impossible. The combination of an iterative method with an adaptive step-size solver is not applicable to SDEs, where the noise in each time step constitutes a random number. However, an iterative approach with fixed step size $\Delta t = h$ is applicable, as long as we ensure that the random noise applied to the neurons remains the same in every iteration. In Sec. 3.2 we investigate the performance of the iterative (Fig. 1B)

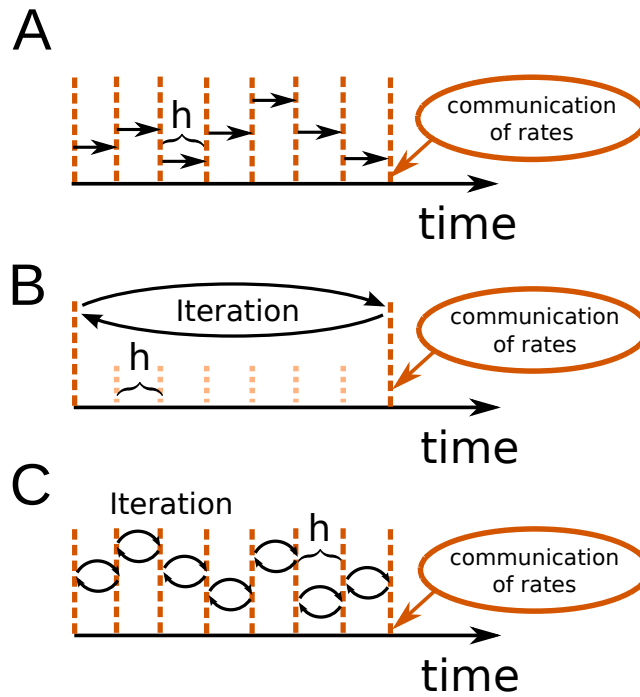


Figure 1: **Different communication strategies for distributed simulations.** Distance between neighboring dotted orange lines indicates computation time step of size h . Distance between neighboring dashed red lines symbolize one communication interval where rates (and other events like spike events) are communicated at the end of the interval. **(A)** Straight-forward solution for rate-based models: rates are communicated in every time step. **(B)** Iterative approach using waveform relaxation: rates are communicated only after $\frac{d_{min}}{h}$ steps and the entire interval is solved repeatedly. **(C)** Iterative approach with communication in every step.

and the standard approach (Fig. 1A) with a focus on large network simulations on supercomputers. In our reference implementation waveform relaxation can be enabled or disabled by a parameter `use_wfr`. Note that in the traditional communication scheme for spiking neuronal networks (Morrison et al., 2005) the first communication occurs earliest at the end of the first update step. Therefore, in the absence of waveform relaxation, the initial input to neurons from the network is omitted.

Fig. 1C shows an alternative iterative approach also feasible within our framework. While this scheme is not needed for the exponential Euler method investigated in the present work, it can be employed to perform a fixed point iteration in order to obtain the solution of the implicit Euler method. However, Sec. 3.1 demonstrates that this is not an efficient option for the integration of rate-based models in distributed simulations.

Table 2 summarizes the parameters of our reference implementation of the waveform-relaxation technique. A subset was previously introduced by Hahne et al. (2015) (`wfr_interpolation_order`, `wfr_max_iterations`, `wfr_tol`), but we rename them here to arrive at more descriptive names. The remaining parameters (`use_wfr`, `wfr_comm_interval`) result from the generalization to rate-based models.

3 Results

In the following, we assess the stability of the different numerical solution schemes and benchmark their performance on large-scale machines. Furthermore, we illustrate the application of the simulation framework to different models relevant in the neuroscientific literature.

3.1 Stability and accuracy of integration methods. To investigate the accuracy and stability of the different numerical methods (see Sec. 2.1) we consider an exactly solvable network of linear rate neurons with $\mu = 0$ (see also Sec. 2.2)

$$\tau dX(t) = A \cdot X(t) dt + \sqrt{\tau} \sigma dW(t). \quad (13)$$

The exact solution of the system of SDEs coincides with the exponential Euler scheme and involves a matrix exponential and a matrix square root (8). This exact solution cannot be obtained with a distributed representation of A as it is typically employed in the distributed simulation scheme of a spiking network simulation code (see Sec. 2.3.1). However, using the methods for numerical matrix computations in MATLAB or Python (both provide an implementation of the same state-of-the-art algorithms, see Al-Mohy & Higham, 2009; Deadman et al., 2012), we obtain an approximation to the exact solution, close to the general limits of floating point

parameter name	type	default	description
<code>use_wfr</code>	bool	true	Boolean parameter to enable (true) or disable (false) the use of the waveform relaxation technique. If disabled and any rate-based neurons (or neurons supporting gap junctions) are present, communication in every step is automatically activated ($d_{\min} = h$).
<code>wfr_comm_interval</code>	double	1.0 ms	Instantaneous rate connections (and gap junctions) contribute to the calculation of the minimal network delay with $\min(d_{\min}, \text{wfr_comm_interval})$. This way the length of the iteration interval of the waveform relaxation can be regulated.
<code>wfr_tol</code>	double	10^{-4}	Convergence criterion for waveform relaxation. The iteration is stopped if the rates of all neurons change less than <code>wfr_tol</code> from one iteration to the next.
<code>wfr_max_iterations</code>	int	15	Maximum number of iterations performed in one application of the waveform relaxation. If the maximum number of iterations has been carried out without reaching the accuracy goal the algorithm advances system time and the reference implementation issues a warning. Additional speed-up in the simulation of rate-based neurons can only be achieved by $\text{wfr_max_iterations} < d_{\min}/h$.
<code>wfr_interpolation_order</code>	int	3	This parameter is exclusively used for gap junctions (see Hahne et al., 2015, Sec. 2.1.2) and has no influence on the simulation of rate-based models.

Table 2: **Parameters of the waveform relaxation algorithm.** The table shows the different parameters of the waveform relaxation algorithm together with their C++ data-type, default value, and a brief description.

numerics, and use this as a reference to compute the root mean square error of the different approximative methods. In order to employ the root mean square error in the context of stochastic differential equations we compute the reference solution for every tested step size and use the same random numbers for both the reference solution and the approximative schemes. Furthermore, we consider analytical stability criteria for some of the employed methods.

In the following we assume that A is diagonalizable, i.e. $A = T^{-1}DT$ with $T = (t^{ij})_{N \times N} \in \mathbb{C}^{N \times N}$ and $D = \text{diag}(\lambda_1, \dots, \lambda_N)$, and transform the system of SDEs with $Z(t) = TX(t)$. It follows

$$\tau dZ(t) = D \cdot Z(t) dt + \sqrt{\tau} \sigma T dW(t)$$

and $Z(t_0) = TX_0$. The transformed system consists of N equations of the form

$$\tau dZ^i(t) = \lambda_i \cdot Z^i(t) dt + \sum_{j=1}^N \sqrt{\tau} \sigma t^{ij} dW^j(t) \quad i = 1, \dots, n \quad (14)$$

that depend on the eigenvalues of A and are independent of each other except for the contribution of the Wiener processes $W^j(t)$. For eigenvalues $\lambda_i \in \mathbb{C}$ with negative real part $\text{Re}(\lambda_i) < 0$, the solution of the i -th transformed equation satisfies

$$|Z^i(t) - \tilde{Z}^i(t)| = e^{\lambda_i(t-t_0)/\tau} |Z_0^i - \tilde{Z}_0^i| < |Z_0^i - \tilde{Z}_0^i|$$

for two different initial values Z_0^i and \tilde{Z}_0^i . It is a desirable stability criterion that a numerical method applied to (13) conserves this property. This is closely related to the concept of A-stability for SDEs (see Kloeden & Platen (1992), Chapter 9.8) and A- respectively B-stability for ODEs (Hairer & Wanner, 1991). A straight-forward calculation shows that the implicit Euler method and the exponential Euler scheme retain this condition regardless of the step size Δt and that the Euler-Maruyama method retains the condition if $|1 + \lambda_i \cdot \Delta t/\tau| < 1$ holds. For $\lambda_i \in \mathbb{R}$ we obtain the step size restriction $\Delta t < \frac{2\tau}{|\lambda_i|}$ and for complex eigenvalues the condition is conserved if $\lambda_i \cdot \Delta t/\tau$ is located inside a unit circle centered at -1 in the complex plane.

We investigate the accuracy of the numerical methods for an all-to-all connected network with inhibitory connections of weight $w^{ij} = \frac{-1}{\sqrt{N}}$. The eigenvalues of $A = -I + \frac{-1}{\sqrt{N}} \cdot \mathbf{1}$ are $\lambda_1 = -1 - \sqrt{N}$ and $\lambda_2 =$

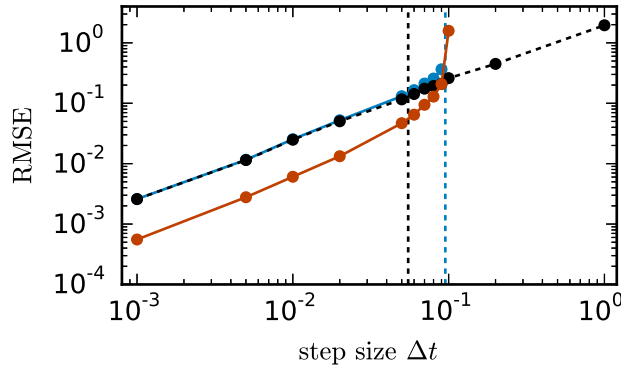


Figure 2: **Comparison of numerical methods for an all-to-all connected inhibitory network.** $\text{RMSE} = \sqrt{\frac{1}{N(t_n - t_0)} \sum_{i=1}^N \sum_{j=1}^n (X_j^i - \hat{X}_j^i)^2}$ of the solution X obtained by the approximate solvers (black dashed curve: implicit Euler method solved with Newton iteration, blue curve: Euler-Maruyama method, red curve: exponential Euler method) with respect to the exact solution \hat{X} as a function of step size in double logarithmic representation. The black vertical line marks the largest step size for which the implicit Euler method solved with fixed-point iteration converges against the one obtained with Newton iteration. The blue vertical line corresponds to the analytical stability restriction $\Delta t \leq \frac{2\tau}{21}$ of the Euler-Maruyama method. Network parameters: size $N = 400$, all-to-all connectivity with $w^{ij} = \frac{-1}{\sqrt{N}}$, $\mu = 0$, $\sigma = 10$ and $\tau = 1$ ms.

... = $\lambda_N = -1$. It follows that the Euler-Maruyama scheme satisfies the stability criterion for $\Delta t \leq \frac{2\tau}{\sqrt{N+1}}$. Fig. 2 shows the root mean square error of the different numerical schemes for an example network. With decreasing step size all investigated methods converge towards the exact solution with convergence order 1, which is consistent with the established theory for SDEs with additive noise (Kloeden & Platen, 1992). The Euler-Maruyama scheme only works within the calculated stability region. The exponential Euler with $A = -I$ and $f(X) = \frac{-1}{\sqrt{N}} \cdot \mathbf{1} \cdot X$, in the following called scalar exponential Euler, shows a similar stability, as the whole input from the network is approximated with an (explicit) Euler-like approach. Within the stability region of Euler-Maruyama, however, the scalar exponential Euler yields more accurate results than the two other methods. The implicit Euler scheme solved with Newton iteration shows no stability issues, but it is not applicable in the distributed simulation framework for spiking neuronal networks (see Sec. 2.3.1). For completeness, we also test the implicit Euler scheme with a parallelizable Jacobi fixed-point iteration. The convergence properties of the fixed-point iteration demand the scheme to be contractive (see e.g. Kelley, 1995, Sec. 4.2). Therefore, in our test case the step size is restricted to roughly $\Delta t < 0.05$ ms and accordingly to a region where the scalar exponential Euler yields better results. In addition, an iterative scheme in each single time step is expected to be much more time consuming than using the scalar exponential Euler scheme. Based on these results we employ the scalar exponential Euler to solve rate-based neuron dynamics (9), as it is the most accurate, stable and efficient scheme compatible with the constraints of the distributed simulation scheme for spiking neural networks. Nevertheless, the inevitable restrictions on the step size Δt need to be taken into account in order to obtain an accurate solution. An appropriate step size can be estimated with the analytical stability criterion of the Euler-Maruyama method. For an all-to-all connected inhibitory network the restriction $\Delta t \leq \frac{2\tau}{\sqrt{N+1}}$ shows that, with increasing network size N or decreasing time constant τ the step size Δt needs to be reduced.

The fully connected network constitutes the worst case test for the class of rate-based models (9), as the absolute value of the negative eigenvalue quickly increases with the number of neurons N . A network which does not suffer from this problem is a perfectly balanced network of excitatory and inhibitory neurons (Rajan & Abbott, 2006). For these models the conditions on the step size Δt of the Euler-Maruyama method are less restrictive and the same is expected for the scalar exponential Euler method. As an example we employ a sparse balanced excitatory-inhibitory-network. In a scaling of the connection weights as $\frac{1}{\sqrt{N}}$, the spectral radius of A and therefore the subsequent stability analysis is independent of N . Fig. 3B demonstrates that for this test case the Euler-Maruyama method is stable for $\Delta t < 1.2\tau$. Given a commonly used simulation step size of $h = \Delta t = 0.1$, networks of this kind can be safely simulated if the time constant τ fulfills $\tau \geq 0.085$.

Random networks with incomplete balance exhibit both types of stability issues discussed above. In this case the matrix A contains an eigenvalue $\lambda_1 = -1 - \rho\sqrt{N}$ which scales with the network size, however, with a proportionality constant $|\rho| < 1$ which is reduced compared to the fully connected inhibitory network and determined by the sparseness and the partial balance. Nevertheless, the network size needs to be taken into account for the choice of the step size. The latter also needs to ensure that the cloud of eigenvalues

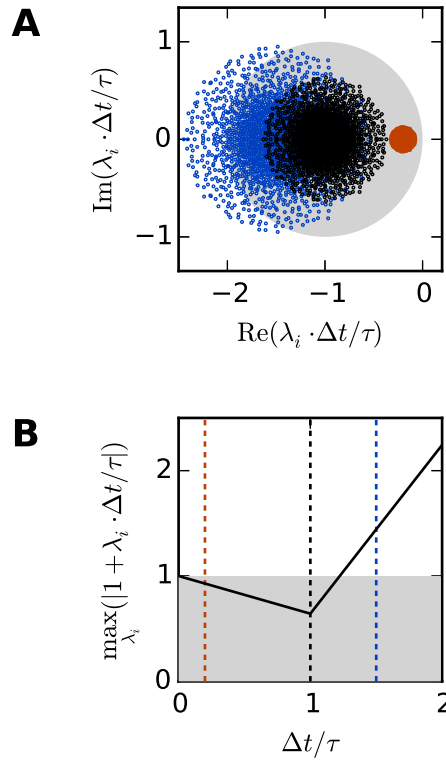


Figure 3: **Stability analysis for a balanced excitatory-inhibitory network.** The network contains in total N neurons where the number of excitatory neurons is four times larger than the number of inhibitory neurons. Each neuron receives input from a fixed number of $0.8 \cdot p \cdot N$ excitatory and $0.2 \cdot p \cdot N$ inhibitory randomly chosen source neurons with connection probability p and connection weights $\frac{1}{\sqrt{N}}$ and $-\frac{4}{\sqrt{N}}$, respectively. **(A)** Black circles show the eigenvalues λ_i of the matrix A for a network of $N = 2000$ neurons. Blue and red circles show the rescaled eigenvalues $\lambda_i \cdot \Delta t / \tau$ for $\Delta t / \tau = 1.5$ and $\Delta t / \tau = 0.2$. The filled gray circle indicates the region where the rescaled eigenvalues $\lambda_i \cdot \Delta t / \tau$ meet the stability criterion $|1 + \lambda_i \cdot \Delta t / \tau| < 1$ of the Euler-Maruyama method. **(B)** The curve shows the maximum of $|1 + \lambda_i \cdot \Delta t / \tau|$ over all eigenvalues λ_i dependent on $\Delta t / \tau$. The gray area again indicates the region where the stability criterion of the Euler Maruyama method is met. Colored vertical lines correspond to the rescaled eigenvalues displayed in panel (A).

determined by the randomness in the connectivity meets the stability criterion.

3.2 Performance of iteration schemes. This section investigates the performance of the rate model implementation. We are interested in i) the scalability of the rate model framework and ii) the comparison between the straight-forward implementation with communication in every computation time step and the iterative approach using waveform relaxation (see Sec. 2.3.3 for details). We perform the simulations on the JUQUEEN BlueGene/Q supercomputer (Jülich Supercomputing Centre, 2015) at the Jülich Research Centre in Germany. It comprises 28,672 compute nodes, each with a 16-core IBM PowerPC A2 processor running at 1.6 GHz. For our benchmarks we use 8 OpenMP threads per JUQUEEN compute node and denote by $\text{VP} = 8 \cdot \#\text{nodes}$ the total number of virtual processes employed.

As a test case we employ the excitatory-inhibitory-network of linear rate neurons ($\phi(x) = \psi(x) = x$) introduced in Sec. 3.1, but with a fixed number of inputs (2000) independent of the number of neurons to allow for an unbiased weak scaling.

A weak scaling (Fig. 4A) shows that the scalability of the straight-forward computation is impaired by the massive amount of communication. While for perfect scaling the simulation time should be constant over the number of virtual processes, the actual simulation time is increased by 15 – 25% when the number of virtual processes is doubled for $\text{VP} < 256$ and even up to 83% from 8,192 to 16,384 virtual processes. For the iterative method, the scaling behavior is close to constant up to 1,024 virtual processes. When more processes are employed, the simulation time is increasing. However, the iterative method shows a better scaling behavior as the increase is weaker compared to the straight-forward computation due to the lower total number of communication steps. Due to the higher computational load of the iterative method (see Sec. 2.3.3) the simulation time is larger compared to the straight forward approach for a small number of VP,

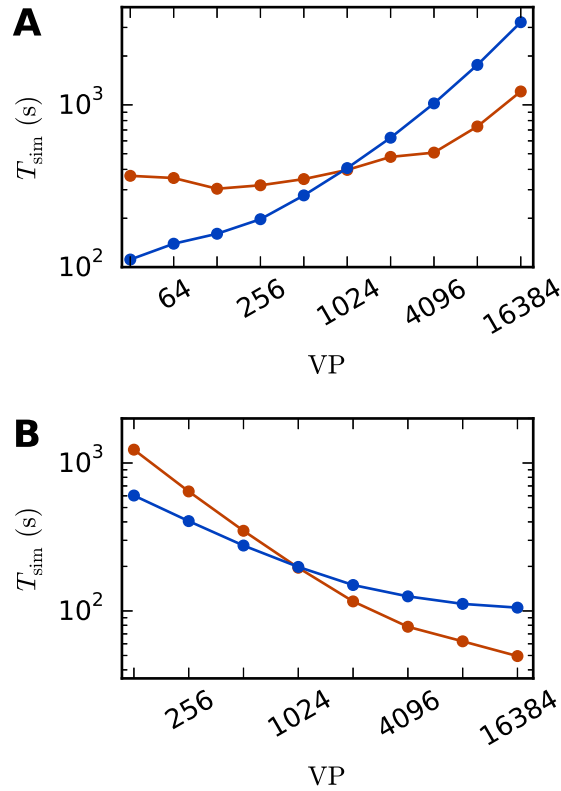


Figure 4: **Scaling behavior of an excitatory-inhibitory network.** Simulation time with waveform relaxation (red curves, `wfr_comm_interval`: 1.0 ms, `wfr_tol`: 10^{-4}) and without waveform relaxation (blue curves) as a function of the number of virtual processes in double logarithmic representation. The simulations span $T = 100$ ms of biological time at a computation step size of $h = 0.1$ ms. **(A)** Weak scaling with 100 neurons per virtual process VP. **(B)** Strong scaling with a total number of $N = 51,200$ neurons. Other network parameters as in Sec. 3.1 with $\mu = 0$, $\sigma = 1$ and $\tau = 10$ ms.

where communication is not that crucial. For $\text{VP} \geq 1024$, the iterative approach is superior with a speed up factor close to three for 16,384 virtual processes (1209 s vs. 3231 s).

The strong scaling scenario with a fixed total number of $N = 51,200$ neurons in Fig. 4B constitutes a similar result. The iterative approach is beneficial for more than 1,024 virtual processes and the scaling behavior of the iterative method outperforms that of the straight-forward computation. Starting at 4,096 virtual processes the savings in computation time decrease, which is explained by the very low workload of each single compute node. Again, for a smaller number of virtual processes the amount of additional computations is too high to outperform the straight-forward computation.

Despite the overall good scaling behavior, the performance in terms of absolute compute time is inferior to a simulator specifically designed for rate-based models alone (not shown). In the latter case it increases performance to collect the states of all neurons in one vector. If further the connectivity is available in form of a matrix and the delays are zero or homogeneous, the network can be efficiently updated with a single matrix-vector multiplication. Thus the increased functionality and flexibility of having rate- and spiking model neurons unified in one simulator comes for the price of a loss of performance for the rate-based models. However, as noted in the introduction, the number of neurons in rate-based network models is usually small and therefore performance is not as critical as for spiking network models.

3.3 Applications. This section presents several applications of the simulation framework. First, we discuss a balanced random network of linear rate units, then include nonlinear neuron dynamics in a random network, and spatially structured connectivity in a functional neural-field model. In each case, simulation results are compared to analytical predictions. Furthermore, we simulate a mean-field model of a spiking model of a cortical microcircuit and discuss possible generalizations.

3.3.1 Linear model. In the asynchronous irregular regime which resembles cortical activity, the dominant contribution to correlations in networks of nonlinear units is given by effective interactions between linear response modes (Grytskyy et al., 2013; Trousdale et al., 2012; Pernice et al., 2011; Dahmen et al., 2016).

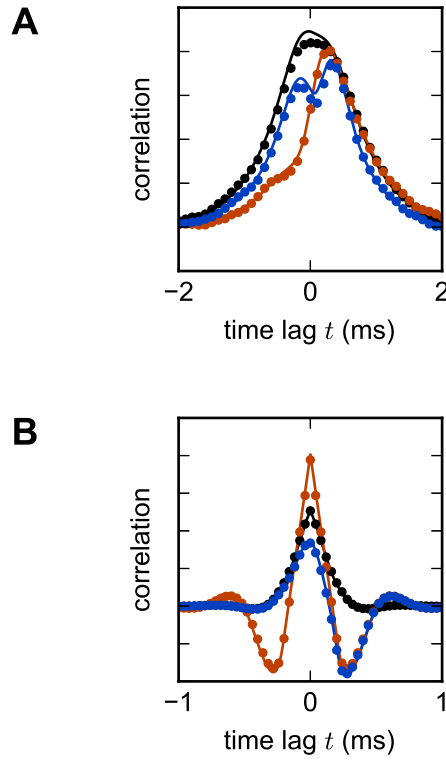


Figure 5: **Linear rate model of a random excitatory-inhibitory network.** **(A)** Cross-correlation functions of two pairs of excitatory neurons (black, red) and an excitatory-inhibitory neuron pair (blue) in a network without delay. The variability across correlation functions arises from heterogeneity in network connections (difference between black and red curves) and from different combinations of cell types (e.g. difference between black and blue curves). **(B)** Population-averaged autocorrelation function for excitatory (black) and inhibitory neurons (red), and cross-correlation function between excitatory and inhibitory neurons (blue) in a network with delay $d = 2$ ms. Symbols denote simulation results, curves show theoretical predictions. Parameters: $N_E = 80$ excitatory and $N_I = 20$ inhibitory neurons, random connections with fixed out-degree, connection probability $p = 0.1$, excitatory weight $w_E = 1/\sqrt{N_E + N_I}$, inhibitory weight $w_I = -6 w_E$, $\tau = 1$ ms, $\mu = 0$, $\sigma = 1$.

Networks of such noisy linear rate models have been investigated to explain features such as oscillations (Bos et al., 2015) or the smallness of average correlations (Tetzlaff et al., 2012; Helias et al., 2013). We here consider a prototypical network model of excitatory and inhibitory neurons following the linear dynamics given by (9) with $\phi(x) = \psi(x) = x$, $\mu = 0$, and noise amplitude σ ,

$$\tau dX^i(t) = \left(-X^i + \sum_{j=1}^N w^{ij} X^j(t) \right) dt + \sqrt{\tau} \sigma dW^i(t). \quad (15)$$

Due to the linearity of the model, the cross-covariance between neurons i and j can be calculated analytically and is given by (Ginzburg & Sompolinsky, 1994; Risken, 1996; Gardiner, 2004; Dahmen et al., 2016)

$$c(t) = \sum_{i,j} \frac{v^{iT} \sigma^2 v^j}{\lambda_i + \lambda_j} u^i u^{jT} \left(\theta(\Delta) \frac{1}{\tau} e^{-\lambda_i \frac{t}{\tau}} + \theta(-\Delta) \frac{1}{\tau} e^{\lambda_j \frac{t}{\tau}} \right), \quad (16)$$

where θ denotes the Heaviside function. The λ_i indicate the eigenvalues of the matrix $1 - W$ corresponding to the i -th left and right eigenvectors v^i and u^i respectively. Non-zero delays yield more complex analytical expressions for cross-correlations. In the population-averaged case, theoretical predictions are still analytically tractable (eq. 18 in Grytskyy et al., 2013). Fig. 5 shows the cross-covariance functions for pairs of instantaneously coupled neurons in a large network, as well as population-averaged covariance functions in a network of excitatory and inhibitory neurons with delayed interactions. In both cases, simulations are in good agreement with the theoretical predictions.

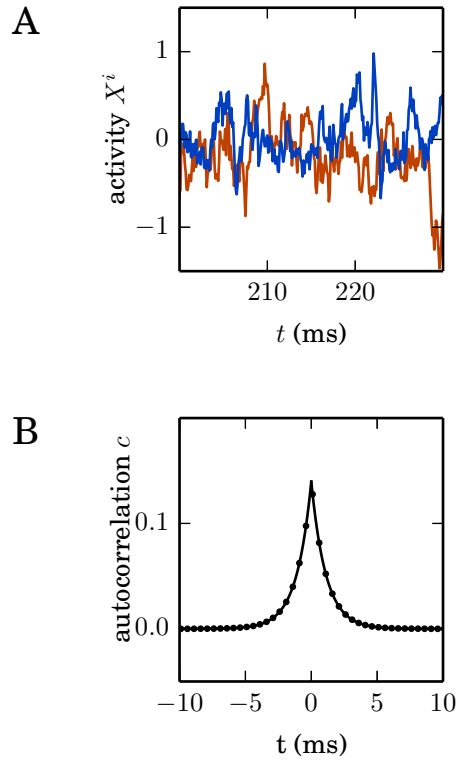


Figure 6: **Nonlinear network model.** Simulation of the network specified by 17 with $N = 1000$ neurons. **(A)** Noisy example trajectories of two neurons. **(B)** Autocorrelation function obtained by simulation averaged over all neurons (dots) and theory (solid curve). Other parameters: $\tau = 1$ ms, $\sigma = 0.5$, $g = 0.5$. Step size as in Fig. 4.

3.3.2 Nonlinear model. So far we considered a network with linear couplings between the units. Qualitatively new features appear in the presence of nonlinearities. One of the most prominent examples is the emergence of chaotic dynamics (Sompolinsky et al., 1988) in a network of non-linearly coupled rate units. The original model is deterministic and has been recently extended to stochastic dynamics (Goedeke et al., 2016). The model definition follows from (9) with $\mu = 0$, $\phi(x) = x$, $\psi(x) = \tanh(x)$, i.e.

$$\tau dX^i(t) = \left(-X^i(t) + \sum_{j=1}^N w^{ij} \tanh(X^j(t)) \right) dt + \sqrt{\tau} \sigma dW^i(t), \quad (17)$$

where $w^{ij} \approx \mathcal{N}(0, g^2/N)$ are Gaussian random couplings. In the thermodynamic limit $N \rightarrow \infty$, the population averaged autocorrelation function $c(t)$ can be determined within dynamic mean-field theory (Sompolinsky et al., 1988; Goedeke et al., 2016; Schuecker et al., 2016). Comparing $c(t)$ obtained by simulation of a network (17) with the analytical result (Goedeke et al., 2016, eqs. 6 and 8) demonstrates excellent agreement (Fig. 6). The simulated network is two orders of magnitude smaller than the cortical microcircuit, illustrating that in this context finite-size effects are already negligible at this scale.

3.3.3 Functional model. Complex dynamics not only arises from nonlinear single-neuron dynamics, but also from structured network connectivity (Yger et al., 2011). One important nonrandom feature of brain connectivity is the spatial organization of connections (Malach et al., 1993; Voges et al., 2010). In spatially structured networks, delays play an essential role in shaping the collective dynamics (Roxin et al., 2005; Voges & Perrinet, 2012). Patterns of activity in such networks are routinely investigated using neural-field models. In contrast to the models discussed above, field models require a discretization of space for numerical simulation. Such discretization can be done in the real space, leading effectively to a network of neurons at discrete positions in space, or alternatively, for particular symmetries in the couplings, in k-space (Roxin et al., 2006). Here, we follow the more general approach of discretization in real space.

A prototypical model of a spatial network is given by (Roxin et al., 2005), where the authors consider the

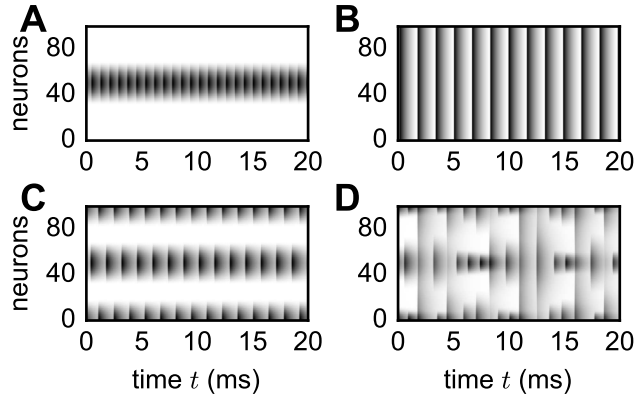


Figure 7: **Spatial patterns in functional neural-field model.** Vertical axis shows neuron indices organized according to ascending angle $\varphi \in [-\pi, \pi)$. Neuronal activity $X_i(t) = X(\varphi_i, t)$ encoded by gray scale with white denoting no activity. Initial transients not shown. Patterns reproduce the analytically derived phase diagram in the original study by Roxin et al. (2005). Parameters: $N = 100$, $d = 0.1$ ms, $\tau = 1$ ms, $I_{\text{ext}} = 1$, $w_0 = -80$, $w_1 = 15$ (A), $w_1 = 5$ (B), $w_1 = -46$ (C), $w_1 = -86$ (D). Initial condition: $X_i(0) = X(\varphi_i, 0) = \pi^2 - \varphi_i^2$.

neural-field model

$$\tau dX(\varphi, t) = \left(-X(\varphi, t) + \phi \left[I_{\text{ext}} + \int_{-\pi}^{\pi} d\varphi' w(|\varphi - \varphi'|) X(\varphi', t - d) \right] \right) dt \quad (18)$$

with delayed (delay d) interactions, constant input I_{ext} , threshold-linear activation function $\phi = x \cdot \theta(x)$ and periodic Mexican-hat shaped connectivity

$$w(|\varphi - \varphi'|) = w_0 + w_1 \cos(\varphi - \varphi'). \quad (19)$$

The spatial variable φ can also be interpreted as the preferred orientation of a set of neurons, thus rendering (18) a model in feature space (Hansel & Sompolinsky, 1998). Discretizing space into N segments yields the following set of coupled ODEs

$$\tau dX^i = \left(-X^i + \phi \left[I_{\text{ext}} + \sum_{j=1}^N w^{ij} X^j(t - d) \right] \right) dt \quad (20)$$

with connectivity $w^{ij} = \frac{2\pi}{N} w(|\varphi^i - \varphi^j|)$, $\varphi_i = -\pi + \frac{2\pi}{N} \cdot i$ for $i \in [1, N]$ and discretization factor $\frac{2\pi}{N}$ that scales the space constants w_0 and w_1 with the neuron density. The spatial connectivity together with a delay in the interaction introduce various spatial activity patterns depending on the shape of the Mexican-hat connectivity. To illustrate applicability of the simulation framework to neural-field models, we reproduce various patterns (Fig. 7) observed by Roxin et al. (2005). Although the discrete and continuous networks strictly coincide only in the thermodynamic limit $N \rightarrow \infty$, numerically obtained patterns shown in Fig. 7 well agree with the analytically derived phase diagram of the continuous model (Roxin et al., 2005) already for network sizes of only $N = 100$ neurons.

3.3.4 Mean-field analysis of complex networks. A network of spiking neurons constitutes a high dimensional and complex system. To investigate its stationary state, one can describe the activity in terms of averages across neurons and time, leading to population averaged stationary firing rates (Brunel, 2000). Here, the spatial average collapses a large number of neurons into a single population, which interpreted as a single rate unit. The ability to represent spiking as well as rate dynamics by the same simulation framework allows a straight-forward analysis of the spiking network by replacing the spiking neuron populations by single rate-based model neurons.

In more formal terms, we now consider networks of neurons structured into N interconnected populations. A neuron in population α receives $K_{\alpha\beta}$ incoming connections from neurons in population β , each with synaptic efficacy $w^{\alpha\beta}$. Additionally, each neuron in population α is driven by $K_{\alpha, \text{ext}}$ Poisson sources with rate X_{ext} and synaptic efficacy w_{ext} . We assume leaky integrate-and-fire model neurons with exponentially decaying post-synaptic currents. The dynamics of membrane potential V and synaptic current I_s is (Fourcaud & Brunel, 2002)

$$\begin{aligned}\tau_m \frac{dV^i}{dt} &= -V^i + I_s^i \\ \tau_s \frac{dI_s^i}{dt} &= -I_s^i + \tau_m \sum_{j=1}^N w^{ij} \sum_k \delta(t - t_k^j - d),\end{aligned}\quad (21)$$

where t_k^j denotes the k -th spike-time of neuron j , and τ_m and τ_s are the time constants of membrane and synapse, respectively. The membrane resistance has been absorbed in the definition of the current. Whenever the membrane potential V crosses the threshold θ , the neuron emits a spike and V is reset to the potential V_r , where it is clamped for a period of length τ_r . If we assume that all neurons have identical parameters, a diffusion approximation leads to the population-averaged firing rates X_α (Fourcaud & Brunel, 2002) :=

$$\begin{aligned}\frac{1}{X_\alpha} &= \tau_r + \tau_m \sqrt{\pi} \int_{(V_r - \mu_\alpha)/\sigma_\alpha + \gamma \sqrt{\tau_s/\tau_m}}^{(\theta - \mu_\alpha)/\sigma_\alpha + \gamma \sqrt{\tau_s/\tau_m}} e^{u^2} (1 + \operatorname{erf}(u)) du \\ &=: 1/\Phi_\alpha(X)\end{aligned}\quad (22)$$

$$\mu_\alpha = \tau_m \sum_{\beta} K_{\alpha\beta} w_{\alpha\beta} X_\beta + \tau_m K_{\alpha,\text{ext}} w_{\text{ext}} X_{\text{ext}}\quad (23)$$

$$\sigma_\alpha^2 = \tau_m \sum_{\beta} K_{\alpha\beta} w_{\alpha\beta}^2 X_\beta + \tau_m K_{\alpha,\text{ext}} w_{\text{ext}}^2 X_{\text{ext}}.\quad (24)$$

Here, $\gamma = |\zeta(1/2)|/\sqrt{2}$, with ζ denoting the Riemann zeta function (Abramowitz & Stegun, 1974). We find the fixed points of (22) by solving the first-order differential equation (Wong & Wang, 2006; Schuecker et al., 2016)

$$\tau dX^\alpha = (-X^\alpha + \Phi(X)) dt,\quad (25)$$

which constitutes a network of rate neurons with the dimension equal to the number of populations N .

Next we apply this framework to a cortical microcircuit model (Potjans & Diesmann, 2014) constituting roughly 80000 spiking neurons structured into 8 populations across 4 layers [$L23$, $L4$, $L5$, $L6$], with one excitatory and one inhibitory cell type each (Fig. 8). The model exhibits irregular and stationary spiking activity (Fig. 8C). Replacing each population by a single rate neuron (8B) results in an eight-dimensional rate network (25) which converges to a fixed point corresponding to the population-averaged firing rates obtained from direct simulation of the spiking model (Fig. 8D).

3.3.5 Further neuron models.

Nonlinear neuron dynamics. A common feature of various rate neurons considered so far is the leaky neuron dynamics, i.e the linear term $-X^i(t)$ in (9). However the presented framework can be easily extended to nonlinear neuron dynamics as used for example by Stern et al. (2014). In a more general form (9) reads

$$\tau dX^i(t) = \left[a(X^i(t)) + \phi \left(\sum_{j=1}^N w^{ij} \psi(X^j(t-d)) \right) \right] dt + \sqrt{\tau} \sigma dW^i(t)\quad (26)$$

where a characterizes the intrinsic neuron dynamics. If a does not contain a linear part, the Euler-Maruyama scheme can be used for the update, i.e.,

$$X_{k+1}^i = X_k^i + \left[a(X_k^i) + \mu + \phi \left(\sum_{j=1}^N w^{ij} \psi \left(X_{k-\frac{d}{\Delta t}}^j \right) \right) \right] \frac{1}{\tau} \Delta t + \frac{1}{\sqrt{\tau}} \sigma \Delta W_k^i.\quad (27)$$

If a also contains a linear part, so that $a(X^i) = -X^i + f(X^i)$, one can use an exponential Euler update approximating the non-linear part as constant during the update. This leads to

$$X_{k+1}^i = e^{-\Delta t/\tau} X_k^i + (1 - e^{-\Delta t/\tau}) \left[f(X_k^i) + \phi \left(\sum_{j=1}^N w^{ij} \psi \left(X_{k-\frac{d}{\Delta t}}^j \right) \right) \right] + \sqrt{\frac{1}{2}(1 - e^{-2\Delta t/\tau})} \sigma \eta_k^i,\quad (28)$$

with $\eta_k^i \sim \mathcal{N}(0, 1)$.

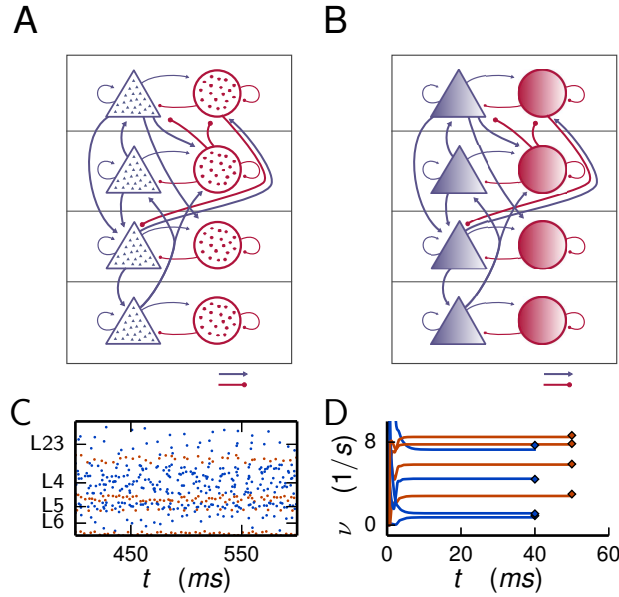


Figure 8: **Reduction of spiking microcircuit model to rate dynamics.** **(A)** Sketch of a microcircuit model (Potjans & Diesmann, 2014) with excitatory (blue triangles) and inhibitory (red circles) neuron populations, each consisting of a large number of neurons indicated by the small triangles and disks respectively. Arrows between populations indicate the in-degree K . **(B)** Sketch of the corresponding reduced model where each population is replaced by a single rate unit. **(C)** Spiking activity in the different layers. **(D)** Dynamics of the eight neurons of the rate network (25) (curves) and comparison to population averaged firing rates obtained from direct simulations of the spiking network (diamonds).

Multiplicative coupling. Another possible extension is a multiplicative coupling between units as for example employed in Gancarz & Grossberg (1998) or the original works of Wilson & Cowan (1972, 1973). In the most general form, this amounts to

$$\tau dX^i(t) = \left[-X^i(t) + H(X^i) \cdot \phi \left(\sum_{j=1}^N w^{ij} \psi(X^j(t-d)) \right) \right] dt + \sqrt{\tau} \sigma dW^i(t), \quad (29)$$

which, again assuming the coupling term to be constant during the update, can be solved using the exponential Euler update

$$X_{k+1}^i = e^{-\Delta t/\tau} X_k^i + (1 - e^{-\Delta t/\tau}) \left[H(X_k^i) \cdot \phi \left(\sum_{j=1}^N w^{ij} \psi \left(X_{k-\frac{d}{\Delta t}}^j \right) \right) \right] + \sqrt{\frac{1}{2}(1 - e^{-2\Delta t/\tau})} \sigma \eta_k^i, \quad (30)$$

with $\eta_k^i \sim \mathcal{N}(0, 1)$.

Multiplicative noise. So far, we have considered rate models subject to additive noise corresponding to $b(t, x(t)) = b(t)$ in (4). The linear rate model considered in Sec. 3.3.1 describes the dynamics around a stationary state and due to the stationary baseline, the noise amplitude is constant. However, one might relax the stationarity assumption which would render the noise amplitude proportional to the time dependent rate, i.e. a multiplicative noise amplitude. The presented framework covers the latter since the exponential Euler update is also valid for multiplicative noise (8).

Output noise. Grytskyy et al. (2013) show that there is a mapping between a network of leaky integrate-and-fire models and a network of linear rate models with so-called output noise. Here the noise is added to the output rate of the afferent neurons

$$\tau \frac{dX^i(t)}{dt} = -X^i(t) + \mu + \phi \left(\sum_{j=1}^N w^{ij} \psi \left(X^j(t-d) + \sqrt{\tau} \sigma \xi^j(t) \right) \right) \quad i = 1, \dots, N \quad (31)$$

and we cannot write the system as a SDE of type (2), as the nonlinearities $\phi(x)$ and $\psi(x)$ are also applied to the white noise ξ^j . In addition to the implementation `rate_neuron_ipn` for the rate-based models (9) discussed

in the present work, our reference implementation also contains a base implementation `rate_neuron_opn` for models with output noise. For these models, the stochastic exponential Euler method can not be employed. Instead the solver assumes the noise ξ^j to be constant over the update interval which leads to the update formula

$$X_{k+1}^i = e^{-\Delta t/\tau} X_k^i + (1 - e^{-\Delta t/\tau}) \left[\mu + \phi \left(\sum_{j=1}^N w^{ij} \psi \left(X_k^j + \sqrt{\frac{\tau}{\Delta t}} \sigma \eta_k^j \right) \right) \right]. \quad (32)$$

The term $X_k^j + \sqrt{\frac{\tau}{\Delta t}} \sigma \eta_k^j$ with $\eta_k^j \sim \mathcal{N}(0, 1)$ is calculated beforehand in the sending neuron j , which results in the same amount of communicated data as in the case of models with input noise.

4 Discussion

This work presents an efficient way to integrate rate-based models in a neuronal network simulator that is originally designed for models with delayed spike-based interactions. The advantage of the latter is a decoupling of neuron dynamics between spike events. This is used by current parallel simulators for large-scale networks of spiking neurons to reduce communications between simulation processes and significantly increase performance and scaling capabilities up to supercomputers (Morrison et al., 2005). In contrast, rate-based models interact in a continuous way. For delayed interactions, neuronal dynamics are still decoupled for the minimal delay of the network such that information can be exchanged on a coarse time-grid. For instantaneous coupling, communication in every time step is required. This is feasible for small networks that can be simulated on small machines and thus require only a small amount of communication. For improved efficiency of simulations of large networks on supercomputers, we implement an iterative numerical solution scheme (Lelarasme, 1982). Furthermore, we investigate several standard methods for the solution of rate model equations and demonstrate that the scalar exponential Euler method is the best choice in the context of a neuronal network simulator that is originally designed for models with delayed spike-based interactions. Afterwards, we show the applicability of the numerical implementation to a variety of well-known and widely-used neuron models (Sec. 3.3) and illustrate possible generalizations to other categories of rate-based neuron models.

The current reference implementation uses an exponential Euler scheme (Adamu, 2011; Komori & Burrage, 2014) with a diagonal matrix A : The additive noise as well as the leaky dynamics of single neurons are exactly integrated while the input to the neurons is approximated as piecewise constant. The analysis in Sec. 3.1 demonstrates that the scalar exponential Euler is the most accurate and stable standard-method for SDEs that is applicable to a distributed spiking simulator. In particular the distributed design renders implicit methods less feasible, as the convergence of the involved fixed-point iteration requires small time-steps in a region where the exponential Euler is already stable and more accurate. As the computation step size needs to be compared against the time constant τ , stable solutions for small values $\tau \ll 1$ may require to decrease the step size below a default value.

The reference implementation provides an optional iterative method, the waveform relaxation (Lelarasme, 1982), for networks with instantaneous rate connections. This method improves scalability by reducing communication at the cost of additional computations. As a consequence, the optimal method (standard vs. iterative) depends on the numbers of compute nodes and virtual processes. In our test case the use of the waveform-relaxation technique is beneficial for 1024 or more virtual processes. It is therefore recommended to employ the iterative scheme for large-scale simulations on supercomputers, but to disable it for smaller rate-model simulations on local workstations or laptops. This can easily be expressed by the parameter `use_wfr` (see Sec. 2.3.3 for details) of the algorithm. In general, the scalability for simulations of rate models is worse than for spiking network simulations (Kunkel et al., 2014) and comparable to simulations with gap junctions (Hahne et al., 2015). This is expected since for rate neurons as well as for gap junctions a large amount of data needs to be communicated compared to a spiking simulation. Future work should assess whether this bottleneck can be overcome by a further optimized communication scheme.

While our reference implementation uses the simulation software NEST as a platform, the employed algorithms can be ported to other parallel spiking network simulators. Furthermore, the implementation of the example neuron models as C++ templates allows easy customization to arbitrary gain functions. Researchers can easily create additional models, without the need for in-depth knowledge of simulator specific data structures or numerical methods. In addition, the developed infrastructure is sufficiently general to allow for extensions to other categories of neuron models as shown explicitly for nonlinear neuron dynamics, multiplicative coupling, and other types of noise. This design enables the usage of the framework for a large body of rate-based neural-network models. Furthermore, the generality of the model equations allows applications beyond neuronal networks, such as e.g. in computational glioscience (Amiri et al., 2012) or artificial intelligence (Haykin, 2009).

Mean-field theory has built a bridge between networks of spiking neurons and rate-based units that either represent single neurons or populations (Buice & Chow, 2007; Buice et al., 2010; Ostojic & Brunel, 2011; Bressloff, 2012; Grytskyy et al., 2013). In the latter case, the rate-based approach comes along with a

considerable reduction of the dimensionality (Sec. 3.3.4). Due to a possibly large number of populations, the fixed-point solution of the stationary activity can generally not be determined analytically, but it can be found by evolving a pseudo-time dynamics. Within the presented framework, this approach is much faster than the spiking counter-part and thus can facilitate calibration of large-scale spiking network models (Schuecker et al., 2016).

The presented unifying framework allows researchers to easily switch between rate-based and spiking neurons in a particular network model requiring only minimal changes to the simulation script. This facilitates an evaluation of the different model types against each other and increases reproducibility in the validation of mean-field reductions of spiking networks to rate-based models. Furthermore, it is instructive to study whether and how the network dynamics changes with the neuron model (Brette, 2015). In particular, functional networks being able to perform a given task are typically designed with rate-based neurons. Their validity can now be evaluated by going from a more abstract rate-based model to a biologically more realistic spiking neuron model. The present reference implementation does not allow for interactions between spiking and rate-based units. While this is technically trivial to implement, the proper conversion from spikes to rates and vice versa is a conceptual issue that has to be explored further by theoretical neuroscience.

The presented joined platform for spike-based and rate-based models hopefully triggers new research questions by facilitating collaboration and translation of ideas between scientists working in the two fields. This work therefore contributes to the unification of both modeling routes in multi-scale approaches combining large-scale spiking networks with functionally inspired rate-based elements to decipher the dynamics of the brain.

5 Appendix

5.1 Numerical evaluation of the Siegert formula. We here describe how to numerically calculate (22), frequently called Siegert formula in the literature (for a recent textbook see Gerstner et al., 2014), which is not straight forward due to numerical instabilities in the integral. First we introduce the abbreviations $y_\theta = (\theta - \mu)/\sigma + \gamma\sqrt{\tau_s/\tau_m}$ and $y_r = (V_r - \mu)/\sigma + \gamma\sqrt{\tau_s/\tau_m}$ and rewrite the integral as

$$\begin{aligned} & \sqrt{\pi} \int_{y_r}^{y_\theta} e^{u^2} (1 + \operatorname{erf}(u)) du \\ &= 2 \int_{y_r}^{y_\theta} e^{u^2} \int_{-\infty}^u e^{-v^2} dv du \\ &= 2 \int_{y_r}^{y_\theta} \int_{-\infty}^u e^{(u+v)(u-v)} dv du. \end{aligned}$$

Here, the numerical difficulty arises due to a multiplication of a divergent (e^{u^2}) and a convergent term ($1 + \operatorname{erf}(u)$) in the integrand. We therefore use the variable transform $w = v - u$ and obtain

$$\begin{aligned} &= 2 \int_{y_r}^{y_\theta} \int_{-\infty}^u e^{(u+v)(u-v)} dv du \\ &= 2 \int_{y_r}^{y_\theta} \int_{-\infty}^0 e^{(2u+w)(-w)} dw du \\ &= \int_0^\infty e^{-w^2} \frac{e^{2y_\theta w} - e^{2y_r w}}{w} dw, \end{aligned}$$

where we performed the integral over u in the last line.

For $y_r, y_\theta < 0$ the integrand can be integrated straightforwardly as

$$\int_0^\infty \frac{e^{2y_\theta w - w^2} - e^{2y_r w - w^2}}{w} dw, \quad (33)$$

where the two terms in the integrand converge separately and where, in approximation, the upper integration bound is chosen, such that the integrand has dropped to a sufficiently small value (here chosen to be 10^{-12}).

Here, for $w = 0$, the integrand has to be replaced by $\lim_{w \rightarrow 0} \frac{e^{2y_\theta w} - e^{2y_r w}}{w} = 2(y_\theta - y_r)$.

For $y_\theta > 0$ and $y_r < 0$ only the combination of the two terms in (33) converges. So we rewrite

$$\begin{aligned} & \int_0^\infty e^{-w^2} \frac{e^{2y_\theta w} - e^{2y_r w}}{w} dw \\ &= \int_0^\infty e^{2y_\theta w - w^2} \frac{1 - e^{2(y_r - y_\theta)w}}{w} dw \\ &= e^{y_\theta^2} \int_0^\infty e^{-(w - y_\theta)^2} \frac{1 - e^{2(y_r - y_\theta)w}}{w} dw. \end{aligned} \quad (34)$$

The integrand has a peak near y_θ . Therefore, in approximation, the lower and the upper boundary can be chosen to be left and right of y_θ , respectively, such that the integrand has fallen to a sufficiently low value (here chosen to be 10^{-12}). For $w = 0$ we replace the integrand by its limit, which is $\lim_{w \rightarrow 0} e^{-(w - y_\theta)^2} \frac{1 - e^{2(y_r - y_\theta)w}}{w} = e^{-y_\theta^2} 2(y_\theta - y_r)$.

We actually switch from (33) to (34) when $y_\theta > 0.05|\tilde{V}_\theta|/\sigma_\alpha$ with $\tilde{V}_\theta = V_\theta + \gamma\sqrt{\tau_s/\tau_m}$. This provides a numerically stable solution in terms of a continuous transition between the two expressions. Our reference implementation numerically evaluates the integrals using the adaptive GSL implementation `gsl_integration_qags` (Galassi et al., 2006) of the Gauss-Kronrod 21-point integration rule.

Conflict of Interest Statement

The authors declare that the research was conducted in the absence of any commercial or financial relationships that could be construed as a potential conflict of interest.

Acknowledgments

The authors gratefully acknowledge the computing time on the supercomputer JUQUEEN (Jülich Supercomputing Centre, 2015) at Forschungszentrum Jülich granted by firstly the JARA-HPC Vergabegremium (provided on the JARA-HPC partition, jinb33) and secondly by the Gauss Centre for Supercomputing (GCS) (provided by the John von Neumann Institute for Computing (NIC) on the GCS share, hwu12). This project has received funding from the European Union's Horizon 2020 research and innovation programme under grant agreement No 720270 (HBP SGA1). Partly supported by Helmholtz Portfolio Supercomputing and Modeling for the Human Brain (SMHB), the Initiative and Networking Fund of the Helmholtz Association, the Helmholtz young investigator group VH-NG-1028, and the Next-Generation Supercomputer Project of MEXT. All network simulations carried out with NEST (<http://www.nest-simulator.org>).

References

- Abbott, L., DePasquale, B., & Memmesheimer, R.-M. (2016). Building functional networks of spiking model neurons. *Nat. Neurosci.* 19(3), 350–355.
- Abramowitz, M., & Stegun, I. A. (1974). *Handbook of Mathematical Functions: with Formulas, Graphs, and Mathematical Tables*. New York: Dover Publications.
- Adamu, I. A. (2011). *Numerical approximation of SDEs and stochastic Swift-Hohenberg equation*. Ph. D. thesis, Heriot-Watt University.
- Al-Mohy, A. H., & Higham, N. J. (2009). A New Scaling and Squaring Algorithm for the Matrix Exponential. *SIAM J. Matrix Analysis Applications* 31(3), 970–989.
- Amari, S.-I. (1977). Dynamics of pattern formation in lateral-inhibition type neural fields. *Biol. Cybern.* 27, 77–87.
- Amiri, M., Bahrami, F., & Janahmadi, M. (2012). Functional contributions of astrocytes in synchronization of a neuronal network model. *Journal of Theoretical Biology* 292, 60 – 70.
- Amit, D. J., & Brunel, N. (1997). Model of global spontaneous activity and local structured activity during delay periods in the cerebral cortex. *Cereb. Cortex* 7, 237–252.
- Bednar, J. A. (2009). Topographica: Building and analyzing map-level simulations from python, c/c++, matlab, nest, or neuron components. *Front Neuroinform.* 24, 8.
- Ben-Yishai, R., Bar-Or, R., & Sompolinsky, H. (1995). Theory of orientation tuning in visual cortex. *Proc. Natl. Acad. Sci. USA* 92, 3844.

- Bogacz, R., Brown, E., Moehlis, J., Holmes, P., & Cohen, J. D. (2006). The physics of optimal decision making: a formal analysis of models of performance in two-alternative forced-choice tasks. *Psychological review* 113(4), 700.
- Bogacz, R., Usher, M., Zhang, J., & McClelland, J. L. (2007). Extending a biologically inspired model of choice: multi-alternatives, nonlinearity and value-based multidimensional choice. *Phil. Trans. R. Soc. B* 362, 1655–1670.
- Bos, H., Diesmann, M., & Helias, M. (2015). Identifying anatomical origins of coexisting oscillations in the cortical microcircuit. *arXiv preprint arXiv:1510.00642*.
- Bos, H., Morrison, A., Peyser, A., Hahne, J., Helias, M., Kunkel, S., Ippen, T., Eppler, J. M., Schmidt, M., Seeholzer, A., Djurfeldt, M., Diaz, S., Morén, J., Deepu, R., Stocco, T., Deger, M., Michler, F., & Plesser, H. E. (2015). *Nest* 2.10.0.
- Bower, J. M., & Beeman, D. (2007). GENESIS (simulation environment). *Scholarpedia* 2(3), 1383.
- Bressloff, P. C. (2012). Spatiotemporal dynamics of continuum neural fields. *Journal of Physics A: Mathematical and Theoretical* 45(3), 033001.
- Bressloff, P. C. (2015). Path-integral methods for analyzing the effects of fluctuations in stochastic hybrid neural networks. *Journal of Mathematical Neuroscience* 5, 4.
- Bressloff, P. C., & Cowan, J. D. (2003). A spherical model for orientation and spatial–frequency tuning in a cortical hypercolumn. *Phil. Trans. R. Soc. B* 358(1438), 1643–1667.
- Bressloff, P. C., Cowan, J. D., Golubitsky, M., Thomas, P. J., & Wiener, M. C. (2001). Geometric visual hallucinations, euclidean symmetry and the functional architecture of striate cortex. *Phil. Trans. R. Soc. B* 356(1407), 299–330.
- Brette, R. (2015). Philosophy of the spike: Rate-based vs. spike-based theories of the brain. *Frontiers in Systems Neuroscience* 9, 151.
- Brette, R., Rudolph, M., Carnevale, T., Hines, M., Beeman, D., Bower, J. M., Diesmann, M., Morrison, A., Goodman, P. H., Harris Jr., F. C., Zirpe, M., Natschläger, T., Pecevski, D., Ermentrout, B., Djurfeldt, M., Lansner, A., Rochel, O., Vieville, T., Muller, E., Davison, A. P., El Boustani, S., & Destexhe, A. (2007). Simulation of networks of spiking neurons: A review of tools and strategies. *J. Comput. Neurosci.* 23(3), 349–398.
- Brunel, N. (2000). Dynamics of sparsely connected networks of excitatory and inhibitory spiking neurons. *J. Comput. Neurosci.* 8(3), 183–208.
- Brunel, N., & Hakim, V. (1999). Fast global oscillations in networks of integrate-and-fire neurons with low firing rates. *Neural Comput.* 11(7), 1621–1671.
- Buice, M. A., & Chow, C. C. (2007). Correlations, fluctuations, and stability of a finite-size network of coupled oscillators. *Phys. Rev. E* 76, 031118.
- Buice, M. A., & Chow, C. C. (2013). Dynamic finite size effects in spiking neural networks. *PLoS Comput Biol* 9(1), 1–21.
- Buice, M. A., & Cowan, J. D. (2007). Field-theoretic approach to fluctuation effects in neural networks. *Phys. Rev. E* 75, 051919.
- Buice, M. A., Cowan, J. D., & Chow, C. C. (2010). Systematic fluctuation expansion for neural network activity equations. *Neural Comput.* 22, 377–426.
- Camperi, M., & Wang, X.-J. (1998). A model of visuospatial working memory in prefrontal cortex: recurrent network and cellular bistability. *J. Comput. Neurosci.* 5(4), 383–405.
- Carnevale, T., & Hines, M. (2006). *The NEURON Book*. Cambridge: Cambridge University Press.
- Chaudhuri, R., Knoblauch, K., Gariel, M.-A., Kennedy, H., & Wang, X.-J. (2015). A large-scale circuit mechanism for hierarchical dynamical processing in the primate cortex. *Neuron* 88(2), 419–431.
- Coombes, S. (2005). Waves, bumps, and patterns in neural field theories. *Biol. Cybern.* 93, 91–108.
- Dahmen, D., Bos, H., & Helias, M. (2016). Correlated fluctuations in strongly coupled binary networks beyond equilibrium. *Phys. Rev. X* 6, 031024.

- De Kamps, M., Baier, V., Drever, J., Dietz, M., Mösenlechner, L., & van der Felde, F. (2008). The state of mind. *Neural Networks* 21(8), 1164–1181.
- Deadman, E., Higham, N. J., & Ralha, R. (2012). Blocked Schur Algorithms for Computing the Matrix Square Root. In P. Manninen & P. Öster (Eds.), *PARA*, Volume 7782 of *Lecture Notes in Computer Science*, pp. 171–182. Springer.
- Deco, G., & Jirsa, V. K. (2012). Ongoing cortical activity at rest: Criticality, multistability, and ghost attractors. *J. Neurosci.* 32(10), 3366–3375.
- Deco, G., Jirsa, V. K., & McIntosh, A. R. (2011). Emerging concepts for the dynamical organization of resting-state activity in the brain. *natrevnscl* 12, 43–56.
- Deco, G., Jirsa, V. K., Robinson, P. A., Breakspear, M., & Friston, K. (2008). The dynamic brain: From spiking neurons to neural masses and cortical fields. *PLoS Comput. Biol.* 4(8), e1000092.
- Destexhe, A., & Paré, D. (1999). Impact of network activity on the integrative properties of neocortical pyramidal neurons in vivo. *J. Neurophysiol.* 81(4), 1531–1547.
- Djurfeldt, M., Lundqvist, M., Johansson, C., Rehn, M., Ekeberg, O., & Lansner, A. (2008). Brain-scale simulation of the neocortex on the IBM Blue Gene/L supercomputer. *IBM Journal of Research and Development* 52(1/2), 31–41.
- Ecker, A. S., Berens, P., Keliris, G. A., Bethge, M., & Logothetis, N. K. (2010). Decorrelated neuronal firing in cortical microcircuits. *Science* 327(5965), 584–587.
- Erlhagen, W., & Schöner, G. (2002). Dynamic field theory of movement preparation. *Psychological review* 109(3), 545.
- Ermentrout, G. B., & Cowan, J. D. (1979). A mathematical theory of visual hallucination patterns. *Biol. Cybern.* 34, 137–150.
- Fan, Z. (2013). Sor waveform relaxation methods for stochastic differential equations. *Appl. Math. Comput.* 219(10), 4992–5003.
- Feldman, J. A., & Ballard, D. H. (1982). Connectionist models and their properties. *Cognitive science* 6(3), 205–254.
- Fourcaud, N., & Brunel, N. (2002). Dynamics of the firing probability of noisy integrate-and-fire neurons. *Neural Comput.* 14, 2057–2110.
- Galassi, M., Davies, J., Theiler, J., Gough, B., Jungman, G., Booth, M., & Rossi, F. (2006). *GNU Scientific Library Reference Manual (2nd Ed.)*. Network Theory Limited.
- Gancarz, G., & Grossberg, S. (1998). A neural model of the saccade generator in the reticular formation. *IEEE Trans. Neural Netw.* 11(7), 1159–1174.
- Gardiner, C. W. (2004). *Handbook of Stochastic Methods for Physics, Chemistry and the Natural Sciences* (3rd ed.). Springer Series in Synergetics. Springer.
- Gentet, L., Avermann, M., Matyas, F., Staiger, J. F., & Petersen, C. C. (2010). Membrane potential dynamics of GABAergic neurons in the barrel cortex of behaving mice. *Neuron* 65, 422–435.
- Gerstner, W., Kistler, W. M., Naud, R., & Paninski, L. (2014). *Neuronal Dynamics. From single Neurons to Networks and Models of Cognition*. Cambridge University Press.
- Gewaltig, M.-O., & Diesmann, M. (2007). NEST (NEural Simulation Tool). *Scholarpedia* 2(4), 1430.
- Ginzburg, I., & Sompolinsky, H. (1994). Theory of correlations in stochastic neural networks. *Phys. Rev. E* 50(4), 3171–3191.
- Goedeke, S., Schuecker, J., & Helias, M. (2016). Noise dynamically suppresses chaos in neural networks. *arXiv preprint arXiv:1603.01880v1*.
- Goodman, D., & Brette, R. (2013). Brian simulator. *Scholarpedia* 8(1), 10883.
- Griffith, J. S., & Horn, G. (1966). An analysis of spontaneous impulse activity of units in the striate cortex of unrestrained cats. *J. Physiol. (Lond.)* 186(3), 516–534.

- Grossberg, S. (1973). Contour enhancement, short term memory, and constancies in reverberating neural networks. *Stud. Appl. Math.* 52(3), 213–257.
- Grytskyy, D., Tetzlaff, T., Diesmann, M., & Helias, M. (2013). A unified view on weakly correlated recurrent networks. *Front. Comput. Neurosci.* 7, 131.
- Hahne, J., Helias, M., Kunkel, S., Igarashi, J., Bolten, M., Frommer, A., & Diesmann, M. (2015). A unified framework for spiking and gap-junction interactions in distributed neuronal network simulations. *Front. Neuroinform.* 9(22).
- Hairer, E., & Wanner, G. (1991). *Solving Ordinary Differential Equations II*. Berlin: Springer.
- Hansel, D., & Sompolinsky, H. (1998). Modeling feature selectivity in local cortical circuits. In C. Koch & I. Segev (Eds.), *Methods in Neuronal Modeling*. Cambridge, Massachusetts: MIT Press.
- Haykin, S. S. (2009). *Neural Networks and Learning Machines* (3rd ed.). Prentice Hall.
- Helias, M., Kunkel, S., Masumoto, G., Igarashi, J., Eppler, J. M., Ishii, S., Fukai, T., Morrison, A., & Diesmann, M. (2012). Supercomputers ready for use as discovery machines for neuroscience. *Front. Neuroinform.* 6, 26.
- Helias, M., Tetzlaff, T., & Diesmann, M. (2013). Echoes in correlated neural systems. *New J. Phys.* 15, 023002.
- Helias, M., Tetzlaff, T., & Diesmann, M. (2014). The correlation structure of local cortical networks intrinsically results from recurrent dynamics. *PLoS Comput. Biol.* 10(1), e1003428.
- Hertz, J., Krogh, A., & Palmer, R. G. (1991). *Introduction to the Theory of Neural Computation*. Perseus Books.
- Hines, M., Eichner, H., & Schürmann, F. (2008). Neuron splitting in compute-bound parallel network simulations enables runtime scaling with twice as many processors. *J Comput Neurosci.* 25(1), 203–210.
- Hines, M., Kumar, S., & Schürmann, F. (2011). Comparison of neuronal spike exchange methods on a Blue Gene/P supercomputer. *Front. Comput. Neurosci.* 5(49). 10.3389/fncom.2011.00049.
- Jülich Supercomputing Centre (2015). JUQUEEN: IBM Blue Gene/Q[®] supercomputer system at the Jülich Supercomputing Centre. *Journal of large-scale research facilities* 1.
- Kelley, C. T. (1995). *Iterative Methods for Linear and Nonlinear Equations*. Number 16 in Frontiers in Applied Mathematics. SIAM.
- Kilpatrick, Z. P. (2014). Wilson-Cowan model. In *Encyclopedia of Computational Neuroscience*. Springer.
- Kloeden, P. E., & Platen, E. (1992). *Numerical Solution of Stochastic Differential Equations*. Berlin: Springer.
- Koch, K. W., & Fuster, J. M. (1989). Unit activity in monkey parietal cortex related to haptic perception and temporary memory. *Exp. Brain Res.* 76(2), 292–306.
- Komori, Y., & Burrage, K. (2014). A stochastic exponential Euler scheme for simulation of stiff biochemical reaction systems. *BIT Numerical Mathematics* 54(4), 1067–1085.
- Kriener, B., Enger, H., Tetzlaff, T., Plesser, H. E., Gewaltig, M.-O., & Einevoll, G. T. (2014). Dynamics of self-sustained asynchronous-irregular activity in random networks of spiking neurons with strong synapses. *Front Comput Neurosci* 8, 136.
- Kumar, S., Heidelberger, P., Chen, D., & Hines, M. (2010). Optimization of applications with non-blocking neighborhood collectives via multisends on the blue gene/p supercomputer. *IPDPD*, 1–11.
- Kunkel, S., Schmidt, M., Eppler, J. M., Masumoto, G., Igarashi, J., Ishii, S., Fukai, T., Morrison, A., Diesmann, M., & Helias, M. (2014). Spiking network simulation code for petascale computers. *Front. Neuroinformatics* 8, 78.
- Laing, C. R., & Chow, C. C. (2002). A spiking neuron model for binocular rivalry. *J. Comput. Neurosci.* 12(1), 39–53.
- Laing, C. R., Troy, W. C., Gutkin, B., & Ermentrout, B. G. (2002). Multiple bumps in a neuronal model of working memory. *SIAM J. Appl. Math.* 63, 62–97.

- Lelarasme, E. (1982). The waveform relaxation method for time domain analysis of large scale integrated circuits: theory and applications. *Memorandum*, No. UCB/ERL M82/40.
- Lindner, B., Doiron, B., & Longtin, A. (2005). Theory of oscillatory firing induced by spatially correlated noise and delayed inhibitory feedback. *Phys. Rev. E* 72, 061919.
- Malach, R., Amir, Y., Harel, M., & Grinvald, A. (1993). Relationship between intrinsic connections and functional architecture revealed by optical imaging and in vivo targeted biocytin injections in primate striate cortex. *Proc. Natl. Acad. Sci. USA* 90, 10469–10473.
- Markram, H., Muller, E., Ramaswamy, S., Reimann, M. W., Abdellah, M., Sanchez, C. A., Ailamaki, A., Alonso-Nanclares, L., Antille, N., Arsever, S., et al. (2015). Reconstruction and simulation of neocortical microcircuitry. *Cell* 163(2), 456–492.
- Mattia, M., & Del Giudice, P. (2002). Population dynamics of interacting spiking neurons. *Phys. Rev. E* 66, 051917.
- Mattia, M., & Del Giudice, P. (2004). Finite-size dynamics of inhibitory and excitatory interacting spiking neurons. *Phys. Rev. E* 70, 052903.
- McClelland, J. L., & Rumelhart, D. E. (1981). An interactive activation model of context effects in letter perception: I. an account of basic findings. *Psychological review* 88(5), 375.
- McClelland, J. L., & Rumelhart, D. E. (1989). *Explorations in parallel distributed processing: A handbook of models, programs, and exercises*. MIT press.
- Miekkala, U., & Nevanlinna, O. (1987). Convergence of dynamic iteration methods for initial value problems. *SIAM J. Sci. and Stat. Comput.* 8(4), 459–482.
- Montbrió, E., Pazó, D., & Roxin, A. (2015). Macroscopic description for networks of spiking neurons. *Phys. Rev. X* 5, 021028.
- Morrison, A., & Diesmann, M. (2008). Maintaining causality in discrete time neuronal network simulations. In P. beim Graben, C. Zhou, M. Thiel, & J. Kurths (Eds.), *Lectures in Supercomputational Neuroscience: Dynamics in Complex Brain Networks*, Understanding Complex Systems, pp. 267–278. Springer.
- Morrison, A., Mehring, C., Geisel, T., Aertsen, A., & Diesmann, M. (2005). Advancing the boundaries of high connectivity network simulation with distributed computing. *Neural Comput.* 17(8), 1776–1801.
- Nichols, E. J., & Hutt, A. (2015). Neural field simulator: two-dimensional spatio-temporal dynamics involving finite transmission speed. *Front. Neuroinform.* 9, 25.
- Ohbayashi, M., Ohki, K., & Miyashita, Y. (2003). Conversion of working memory to motor sequence in the monkey premotor cortex. *Science* 301(5630), 233–236.
- Okun, M., & Lampl, I. (2008). Instantaneous correlation of excitation and inhibition during ongoing and sensory-evoked activities. *Nat. Neurosci.* 11(5), 535–537.
- O'Reilly, R. C. (2014). Comparison of neural network simulators. https://grey.colorado.edu/emergent/index.php/Comparison_of_Neural_Network_Simulators. Accessed: 2016-10-14.
- O'Reilly, R. C., Munakata, Y., Frank, M. J., Hazy, T. E., & Contributors (2012). *Computational Cognitive Neuroscience*. Wiki Book, 1st Edition, URL: <http://ccnbook.colorado.edu>.
- O'Reilly, R. C., Munakata, Y., & McClelland, J. L. (2000). *Computational Explorations in Cognitive Neuroscience: Understanding the Mind by Simulating the Brain* (1 ed.). MIT Press.
- Ostojic, S. (2014). Two types of asynchronous activity in networks of excitatory and inhibitory spiking neurons. *Nat. Neurosci.* 17, 594–600.
- Ostojic, S., & Brunel, N. (2011). From spiking neuron models to linear-nonlinear models. *PLoS Comput. Biol.* 7(1), e1001056.
- Pernice, V., Staude, B., Cardanobile, S., & Rotter, S. (2011). How structure determines correlations in neuronal networks. *PLoS Comput. Biol.* 7(5), e1002059.
- Plesser, H., Diesmann, M., Gewaltig, M.-O., & Morrison, A. (2015). Nest: the neural simulation tool. In D. Jaeger & R. Jung (Eds.), *Encyclopedia of Computational Neuroscience*, pp. 1849–1852. Springer New York.

- Plotnikov, D., Blundell, I., Ippen, T., Eppler, J. M., Morrison, A., & Rumpe, B. (2016). NESTML: a modeling language for spiking neurons. In *Modellierung 2016 Conference*, Volume 254 of *LNI*, pp. 93–108. Bonner Köllen Verlag.
- Potjans, T. C., & Diesmann, M. (2014). The cell-type specific cortical microcircuit: Relating structure and activity in a full-scale spiking network model. *Cereb. Cortex* 24(3), 785–806.
- Rajan, K., & Abbott, L. F. (2006). Eigenvalue spectra of random matrices for neural networks. *Phys. Rev. Lett.* 97, 188104.
- Renart, A., De La Rocha, J., Bartho, P., Hollender, L., Parga, N., Reyes, A., & Harris, K. D. (2010). The asynchronous state in cortical circuits. *Science* 327, 587–590.
- Risken, H. (1996). *The Fokker-Planck Equation*. Springer Verlag Berlin Heidelberg.
- Rougier, N. P., & Fix, J. (2012). Dana: Distributed numerical and adaptive modelling framework. *Network: Computation in Neural Systems* 23(4), 237–253.
- Roxin, A., Brunel, N., & Hansel, D. (2005). The role of delays in shaping spatio-temporal dynamics of neuronal activity in large networks. *Phys. Rev. Lett.* 94(23), 238103.
- Roxin, A., Brunel, N., & Hansel, D. (2006). Rate Models with Delays and the Dynamics of Large Networks of Spiking Neurons. *Progress of Theoretical Physics Supplement* 161, 68–85.
- Roxin, A., Brunel, N., Hansel, D., Mongillo, G., & van Vreeswijk, C. (2011). On the distribution of firing rates in networks of cortical neurons. *J. Neurosci.* 31(45), 16217–16226.
- Rumelhart, D. E., McClelland, J. L., & the PDP Research Group (1986). *Parallel Distributed Processing, Explorations in the Microstructure of Cognition: Foundations*, Volume 1. Cambridge, Massachusetts: MIT Press.
- Samsonovich, A., & McNaughton, B. L. (1997). Path integration and cognitive mapping in a continuous attractor neural network model. *J. Neurosci.* 17(15), 5900–5920.
- Sanz Leon, P., Knock, S., Woodman, M., Domide, L., Mersmann, J., McIntosh, A., & Jirsa, V. (2013). The virtual brain: a simulator of primate brain network dynamics. *Front. Neuroinform.* 7, 10.
- Schmidt, M., Bakker, R., Diesmann, M., & van Albada, S. (2016). Full-density multi-scale account of structure and dynamics of macaque visual cortex. *arXiv preprint arXiv:1511.09364v3*.
- Schöner, G., Spencer, J., & Group, D. (2015). *Dynamic Thinking: A Primer on Dynamic Field Theory*. Oxford Series in Developmental Cognitive Neuroscience. Oxford University Press.
- Schuecker, J., Diesmann, M., & Helias, M. (2015). Modulated escape from a metastable state driven by colored noise. *Phys. Rev. E* 92, 052119.
- Schuecker, J., Goedeke, S., Dahmen, D., & Helias, M. (2016). Functional methods for disordered neural networks. *arXiv*, 1605.06758.
- Schuecker, J., Schmidt, M., van Albada, S., Diesmann, M., & Helias, M. (2016). Fundamental activity constraints lead to specific interpretations of the connectome. *arXiv preprint arXiv:1509.03162v3*.
- Schurz, H., & Schneider, K. R. (2005). Waveform relaxation methods for stochastic differential equations. *International Journal of Numerical Analysis and Modeling* 3(2), 232–254.
- Shadlen, M. N., & Newsome, W. T. (1998). The variable discharge of cortical neurons: Implications for connectivity, computation, and information coding. *J. Neurosci.* 18(10), 3870–3896.
- Shoji, I. (2011). A note on convergence rate of a linearization method for the discretization of stochastic differential equations. *Communications in Nonlinear Science and Numerical Simulation* 16(7), 2667–2671.
- Siebert, A. J. (1951). On the first passage time probability problem. *Phys. Rev.* 81(4), 617–623.
- Softky, W. R., & Koch, C. (1993). The highly irregular firing of cortical cells is inconsistent with temporal integration of random EPSPs. *J. Neurosci.* 13(1), 334–350.
- Sompolinsky, H., Crisanti, A., & Sommers, H. J. (1988). Chaos in random neural networks. *Phys. Rev. Lett.* 61, 259–262.

- Stern, M., Sompolinsky, H., & Abbott, L. F. (2014). Dynamics of random neural networks with bistable units. *Phys. Rev. E* 90, 062710.
- Stevens, J.-L. R., Law, J. S., Antolík, J., & Bednar, J. A. (2013). Mechanisms for stable, robust, and adaptive development of orientation maps in the primary visual cortex. *J. Neurosci.* 33(40), 15747–15766.
- Tetzlaff, T., Helias, M., Einevoll, G., & Diesmann, M. (2012). Decorrelation of neural-network activity by inhibitory feedback. *PLoS Comput. Biol.* 8(8), e1002596.
- Trousdale, J., Hu, Y., Shea-Brown, E., & Josic, K. (2012). Impact of network structure and cellular response on spike time correlations. *PLoS Comput. Biol.* 8(3), e1002408.
- Usher, M., & McClelland, J. L. (2001). The time course of perceptual choice: the leaky, competing accumulator model. *Psychological review* 108(3), 550.
- van Albada, S. J., Helias, M., & Diesmann, M. (2015). Scalability of asynchronous networks is limited by one-to-one mapping between effective connectivity and correlations. *PLoS Comput. Biol.* 11(9), e1004490.
- van Vreeswijk, C., & Sompolinsky, H. (1996). Chaos in neuronal networks with balanced excitatory and inhibitory activity. *Science* 274, 1724–1726.
- Voges, N., & Perrinet, L. U. (2012). Complex dynamics in recurrent cortical networks based on spatially realistic connectivities. *Front. Comput. Neurosci.* 6, 41.
- Voges, N., Schüz, A., Aertsen, A., & Rotter, S. (2010). A modeler's view on the spatial structure of intrinsic horizontal connectivity in the neocortex. *Prog. Neurobiol.* 92(3), 277–292.
- Weitzenfeld, A., Arbib, M. A., & Alexander, A. (2002). *The neural simulation language: A system for brain modeling*. MIT Press.
- Wilson, H. R. (2003). Computational evidence for a rivalry hierarchy in vision. *Proc. Natl. Acad. Sci. USA* 100(24), 14499–14503.
- Wilson, H. R., & Cowan, J. D. (1972). Excitatory and inhibitory interactions in localized populations of model neurons. *Biophys. J.* 12(1), 1–24.
- Wilson, H. R., & Cowan, J. D. (1973). A mathematical theory of the functional dynamics of cortical and thalamic nervous tissue. *Kybernetik* 13, 55–80.
- Wong, K.-F., & Wang, X.-J. (2006). A recurrent network mechanism of time integration in perceptual decisions. *J. Neurosci.* 26(4), 1314–1328.
- Yger, P., El Boustani, S., Destexhe, A., & Frégnac, Y. (2011). Topologically invariant macroscopic statistics in balanced networks of conductance-based integrate-and-fire neurons. *J. Comput. Neurosci.* 31, 229–245.